Cassini's geological and compositional view of Tethys

Katrin Stephan, Roland Wagner, Ralf Jaumann, Roger Clark, Dale Cruikshank, Robert Brown, Bernd Giese, Thomas Roatsch, Gianrico Filacchione, Dennis Matson, et al.

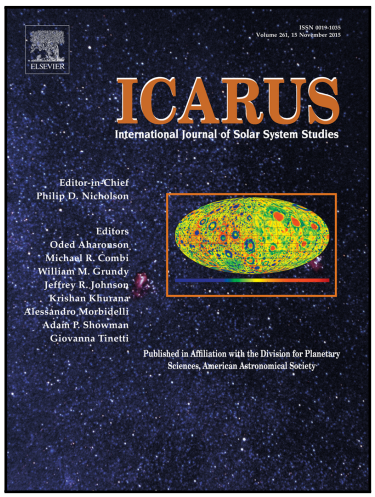

Cassini's geological and compositional view of Tethys

Katrin Stephan , Roland Wagner , Ralf Jaumann , RogerN. Clark , DaleP. Cruikshank , RobertH. Brown , Bernd Giese , Thomas Roatsch , Gianrico Filacchione , Dennis Matson , CristinaDalle Ore , Fabrizio Capaccioni , KevinH. Baines , Sebastian Rodriguez , Norbert Krupp , BonnieJ. Buratti , PhilD. Nicholson

PII: S0019-1035(16)00136-6
DOI: 10.1016/j.icarus.2016.03.002
Reference: YICAR 11977

To appear in: *Icarus*

Received date: 10 November 2015
Revised date: 7 March 2016
Accepted date: 8 March 2016

Please cite this article as: Katrin Stephan , Roland Wagner , Ralf Jaumann , RogerN. Clark , DaleP. Cruikshank , RobertH. Brown , Bernd Giese , Thomas Roatsch , Gianrico Filacchione , Dennis Matson , CristinaDalle Ore , Fabrizio Capaccioni , KevinH. Baines , Sebastian Rodriguez , Norbert Krupp , BonnieJ. Buratti , PhilD. Nicholson , Cassini's geological and compositional view of Tethys, *Icarus* (2016), doi: 10.1016/j.icarus.2016.03.002

Highlights

- Tethys exhibits spectral variations unique in the Saturnian system.
- The formation of Ithaca Chasma is not related to the Odysseus impact event.
- Odysseus might be responsible for N-S trending 'icy' bands of large ice particles.
- Fresh surface material on Tethys exhibits a similar composition like Dione and Rhea.
- The crusts of Tethys, Dione and Rhea have similar chemical/physical properties.

Cassini's geological and compositional view of Tethys

Katrin Stephan[1], Roland Wagner[1], Ralf Jaumann[1,2], Roger N. Clark[3], Dale P. Cruikshank[4], Robert H. Brown[5], Bernd Giese[1], Thomas Roatsch[1], Gianrico Filacchione[6], Dennis Matson[7], Cristina Dalle Ore[4], Fabrizio Capaccioni[6], Kevin H. Baines[8], Sebastian Rodriguez[9], Norbert Krupp[10], Bonnie J. Buratti[6] and Phil D. Nicholson[11]

[1] *DLR, Institute of Planetary Research, 12489 Berlin, Germany;*

[2] *Dept. of Earth Sciences, Inst. of Geosciences, Free University, Berlin, Germany;*

[3] *U.S. Geological Survey, Denver Federal Center, Denver, CO 80225, USA;*

[4] *NASA Ames Research Center, Moffett Field, CA 94035, USA;*

[5] *Lunar and Planetary Laboratory, University of Arizona, Tucson, AZ 85721, USA;*

[6] *INAF-IAPS, 00133 Rome, Italy;*

[7] *Jet Propulsion Laboratory, California Institute of Technology, Pasadena, CA 91109, USA;*

[8] *Space Science and Engineering Center, University of Wisconsin-Madison, Madison, WI 53706, USA;*

[9] *Université Paris-Diderot, 75013 Paris, France;*

[10] *Max-Planck-Institut für Sonnensystemforschung, 37077 Göttingen;*

[11] *Department of Astronomy, Cornell University, Ithaca, NY 14853, USA;*

Running Title: Tethys' geological and spectral properties [<50 characters]

Abstract

[<250 words]

The Saturnian satellite Tethys exhibits geological and spectral properties, whose appearance, nature and spatial distribution partly mirror those identified on the neighboring satellites Dione and Rhea or fit to the picture how spectral surface properties are expected to change from one satellite to the other within the inner Saturnian system. However, we also identified spectral variations that are unique in the Saturnian system. Whereas geologically young surface features are characterized by pure H_2O-ice composition with relatively large particles, which match the particle sizes measured for fresh surface features also on Dione and Rhea, geologically old weathered regions are dominated by submicron-sized ice particles. Our investigations confirm that the Odysseus impact event did not cause the formation of Tethys' extended graben system Ithaca Chasma. On the contrary, Odysseus might be responsible for the N-S trending 'icy' bands that mark Tethys' surface in the center of its leading and trailing hemisphere.

Keywords

Cassini, VIMS, Tethys, surface composition, geology

1 Introduction

Since 2004 Cassini has been orbiting the Saturnian system with its instruments detecting the chemical and physical properties of Saturn's atmosphere, magnetosphere, satellites, and rings. The VIMS instrument is the first imaging spectrometer that operates in the Saturnian system, enabling not only the identification of the surface composition but also the mapping of its distribution on the surfaces of Saturn's satellites. Spectral analyses of Dione, Rhea, Iapetus, Hyperion [*Clark et al.*, 2008; *Clark et al.*, 2012; *Cruikshank et al.*, 2007; *Stephan et al.*, 2010; *Stephan et al.*, 2012] and Enceladus [*Jaumann et al.*, 2008] have made it possible to relate location and extension of spectral units to specific geological and/or geomorphological surface features or characteristics of the space environment – which is essential to resolve the origin of the surface compounds and thus provides valuable information to describe the evolution of the satellite. Although the VIMS spectra of the icy satellites' surfaces are mostly dominated by H_2O-ice, its distribution and physical characteristics differ distinctly from one satellite to the other [*Clark et al.*, 2008; *Clark et al.*, 2012; *Jaumann et al.*, 2008; *Stephan et al.*, 2010; *Stephan et al.*, 2012]. Global hemispherical differences are mostly related to the satellite's position in the Saturnian system, i.e., the distance to Saturn and/or its E ring, with particles trapped in Saturn's magnetosphere and/or ice grains of the E ring impacting their surfaces [*Clark et al.*, 2008; *Stephan et al.*, 2010; *Stephan et al.*, 2012]. Thanks to VIMS mapping capabilities, compositional variations on a regional and local scale can be identified and related to the surface geology. In particular, young or reactivated impact craters and tectonic features – revealing "fresh" (unaltered) surface material - offer a unique view into the crustal properties of the satellite [*Stephan et al.*, 2010; *Stephan et al.*, 2012]. Furthermore, the comparison of the physical and chemical surface properties of impact craters emplaced at

different times enables to study the alteration of the surface material due to space weathering processes.

In this paper we present the analysis of the spectral properties of Tethys in comparison to its geology, which is unique in several ways and completes our investigation of Saturn's inner major satellites. Tethys is 1,062 km in diameter and exhibits a very low density (~0.985 g/cm^3) [*Thomas*, 2010] suggesting that the satellite is composed almost entirely of H_2O ice plus a small amount of rock.

Tethys is marked by the huge impact basin Odysseus, which is expected to have globally affected surface and internal properties. Odysseus is still discussed as being responsible for the formation of Tethys' prominent tectonic system, Ithaca Chasma [*Moore and Ahern*, 1983; *J M Moore et al.*, 2004]. Surface ages, however, indicate that Ithaca Chasma is geologically older than Odysseus [*Giese et al.*, 2007] – speaking against this relationship. Further, the impact crater statistics, at the basis of Tethys' surface age calculations, are unusual. The distribution of small impact craters (1 to 10 km in diameter) is distinctly different from the other Saturnian satellites because the number of these small impact craters is much higher relative to the larger ones [*Schmedemann et al.*, 2014].

Finally Tethys has a high albedo value of about 0.8 in the visual spectral range [*Verbiscer et al.*, 2007] indicating a composition largely made of H_2O ice. Possibly, the high reflectivity is enhanced because Tethys collects Saturn's E-ring H_2O-ice particles generated by geysers on Enceladus. Tethys orbits Saturn at a distance of 294,660 kilometers, between the orbits of Enceladus and Dione, and is thus embedded in the E ring environment. Consequently, the comparison of the compositional aspects of all Saturnian satellites provides valuable information for the evolution of the Saturnian system.

Key questions about Tethys upon which this investigation is focused to unravel include:

1. How are Odysseus and Ithaca Chasma spectrally characterized? How are they related to each other in general? Do the spectral surface properties provide any hint of a common origin and their relation to the history and formation of the body?
2. Are there any fresh impact craters on Tethys? What are the similarities and differences in the spectral properties of fresh surface features on Tethys compared to fresh impact craters on Dione (Creusa) and Rhea (Inktomi)?
3. What are the differences in spectral properties between any fresh surface material and the surroundings? What are the resurfacing dynamics and space weathering effects of the satellite?
4. Are there any hemispherical changes in the spectral properties similar to Dione and Rhea related to the interaction with Saturn's magnetosphere? How do they change from one satellite to the other? What information do they give about the properties of Saturns magnetosphere?
5. How do the E ring particles interact with Tethys, which orbits relatively close to the E ring?

We start the presentation of our work with an overview of the data set we used (section 2), including the methods used for the spectral and geological analysis. Sections 3 and 4 present the achieved results. In section 3 the identified major geological units are described in detail. In section 4 Tethys spectral properties and the distribution of spectrally different units across Tethys' surface as well as their possible associations to specific geological – and/or geomorphological features or location on Tethys's surface are discussed. The possible implications for the origin/formation of Tethys' surface compounds and Tethys' geological evolution are discussed in section 5 and summarized in section 6.

2 Cassini data basis

Since 2004, the Cassini spacecraft has been orbiting the Saturnian system exploring Saturn, its magnetosphere and its satellites with numerous flybys at Tethys (Tab. 1). Cassini performed 10 (1 targeted and 9 non-targeted) flybys during its nominal mission until 2008, with an altitude between 1500 and about 120,000 km. In particular, Cassini's orbit 47 offered the unique possibility to observe Ithaca Chasma, Tethys' most prominent tectonic features (see below) from a distance of only 16,000 km. Throughout the first extended mission, the Cassini Equinox Mission, from 2009 and 2010, more data were collected during 11 flybys with a closest approach of about 37,000 km during orbit 136, which mainly observed Tethys' trailing hemisphere. In the current second extended mission, the Cassini Solstice Mission, which will continue until 2017, already 7 flybys within distances between about 7600 and 69,000km were successfully performed so far, with orbit 168 offering the possibility to investigate Tethys' largest impact crater Odysseus.

2.1 ISS observations

Spatially highly resolved Clear filter images acquired by the Imaging Science Subsystem (ISS) provided not only the geological context but provided the possibility to associate any changes in the spectral properties to specific geographic location, as well as individual geological and/or geomorphological surface features.

A digital global mosaic in a simple-cylindrical map-projection of Tethys produced with Clear filter images of the Cassini ISS instrument with a map scale of 0.29 km/pixel, as presented in *Roatsch et al.* [2009], was used for the global geological mapping procedure as well as the comparison to Tethys' global spectral surface properties. For this purpose we rescaled the mosaic to a lower map scale of 1 km/pixel, which is sufficient for comparison with the global VIMS map since the latter have generally a lower pixel ground resolution than the ISS

images. This is the same approach as used for our geologic mapping of Dione and Rhea [*Stephan et al.*, 2010; *Stephan et al.*, 2012]. A map scale of 1 km/pixel is also sufficient to identify global geologic units, individual units within major impact structures. In order to constrain the location of geologic boundaries and in order to characterize a geologic unit as well as to support the investigation of local geological and spectral properties of Tethys, however, we also used the original higher-resolution imaging data to support the mapping procedure. Furthermore, in order to prevent a misinterpretation of VIMS signal due to viewing conditions [*Stephan et al.*, 2012] at the time of the acquisition, simultaneously acquired ISS images were used for comparison.

Although not exclusively designed for the development of digital terrain models (DTMs), individual images provide the opportunity to produce DTMs of regional areas using the stereo-technique like the DTM of Ithaca Chasma already presented in the work of *Giese et al.* [2007]. Previous works [*Stephan et al.*, 2014; *Stephan et al.*, 2012] showed the potential in the possibility to associate spectral properties to local topographic changes like slopes, etc., especially in tectonically formed regions.

2.2 VIMS observations

VIMS consists of two instruments that measure sunlight reflected from the surfaces of the satellites. They generate image cubes in which each pixel represents a spectrum consisting of 352 contiguous spectral channels [*Brown et al.*, 2004]. The VIMS V instrument possesses 96 spectral channels that measure radiation between 0.35 and 1.05 mm, while the VIMS IR instrument operates between 0.86 to 5.2 mm and collects light in 256 spectral channels. The spectral sampling intervals of VIMS V and VIMS IR is 8 and 16 nm, respectively, which is sufficient to analyze absorptions (their wavelength position, shape and band depth) of H_2O-ice

at 1.04, 1.25, 1.5 and 2 μm. The dynamic range of 12 bit (2^{12}=4096 values) makes it possible to measure relatively small variations in the band depth of the specific absorptions.

Possessing an Instantaneous Field Of View (IFOV) of 0.5 mrad in the nominal operation mode enables spectral images with resolutions sufficient for conducting detailed spatial analyses of the spectral characteristics of the surface [*Brown et al.*, 2004; *Stephan et al.*, 2012].

VIMS observations were chosen depending on coverage, pixel ground resolution and illumination conditions. These parameters differ significantly during each VIMS observation sequence. Table 1 summarizes the Cassini flybys offering VIMS data incorporated into our analysis. VIMS observations with pixel ground resolutions of better than 100 km per pixel cover most of Tethys' surface except the northern polar region (Fig.1). Pixel ground resolutions up to 50 km enable at least a global view of Tethys' geological and spectral properties, such as hemispherical differences. VIMS observations exhibiting pixel ground resolution between 50 and 20 km per pixel offer the analysis of any regional relationships. VIMS data for Ithaca Chasma region, acquired during Cassini's 47th orbit in June, 2007, exhibit pixel ground resolution of better than 20 km/pixel and cover the canyon system between 60°S and 80°N. Furthermore, during several flybys (Cassini orbits 94, 119, 136, 164 and 214) in the "Equinox" mission (2009 - 2010) and in the recent Cassini Solstice Mission (2010-2017) VIMS has acquired data showing us a unique view of Tethys' trailing hemisphere. During orbit 168 (Cassini Solstice Mission) VIMS observations revealed details of Tethys' impact crater Odysseus (32.8°N/128.9°W) on the satellite's leading hemisphere, which, with a diameter of 445 km is the largest impact crater on this body. Unfortunately, being at the terminator, Odysseus was not fully illuminated during the acquisition. As a consequence of this, the western portion of the crater is hidden on the night side. Most of the

VIMS observations exhibit phase angles smaller than 60° (Fig.1), which are sufficient for the spectral analysis, cover most of Tethys surface (see below).

[Figure 1]

[Table 1]

2.3 Processing and Spectral Analysis of VIMS data

VIMS data were radiometrically calibrated, i.e., converted from raw data numbers (*DN*) into physical values of reflectance (*I/F*) by the VIMS team using the latest instrument's spectro-radiometric response function [*Brown et al.*, 2004; *Stephan et al.*, 2010]. In order to attribute variations in the spectral properties to the corresponding geographic locations and to combine the VIMS data set with the Cassini ISS base map [*Roatsch et al.*, 2009] and individual ISS images, each individual VIMS cube is geometrically re-projected, converted into a map-projected VIMS cube following the procedure described in detail by *Jaumann et al.* [2006], and finally combined into a global Tethys VIMS mosaic that fits the global ISS base map. Since our applied mosaicking procedure also allows arranging the incorporated individual observations depending on coverage, spatial resolution and quality (including S/N ratio, phase angle and/or saturation effects) influences of VIMS observations with lower spatial resolution (>60 km per pixel), phase angles larger than 60° as well as saturation effects, which frequently occurred in the wavelength region between 1 and 1.4µm onto the quality of the spectral maps are minimized.

Like most of the Saturnian satellites, Tethys' surface is substantially covered by H_2O-ice, the main focus of this study. Its major absorption bands at 1.04, 1.25, 1.5, 2, 3 and 4.5µm

dominate every VIMS spectrum. These H_2O-ice absorptions are known to be sensitive to abundance, size and crystallinity of the ice particles, affecting the slope of spectral continuum, the depth and wavelength position of these absorptions. Our goal is to measure the individual spectral parameters of H_2O-ice in the VIMS spectra and map their variations across Tethys' surface on a pixel by pixel basis in order to investigate the observed pattern with respect to possible associations to a specific location and/or geological and morphological surface features, which is essential for resolving the processes responsible for their formation. We concentrate the spectral analysis on specific spectral parameters of the H_2O-ice spectrum, which were already successfully used for the spectral analysis of icy satellites' surfaces [*Clark et al.*, 2008; *Jaumann et al.*, 2008; *Stephan et al.*, 2010; *Stephan et al.*, 2012]. Because the absorptions at 3 and 4.5µm are always spectrally saturated we focus on the H_2O-ice absorption bands occurring between 1 and 3µm. In order to compare the spectral properties of Tethys to the previous analyses done for Enceladus, Dione, and Rhea we use the same tools for identifying and mapping existing absorption features, i.e. their spectral parameters like wavelength position and depth [*Jaumann et al.*, 2008; *Stephan et al.*, 2010; *Stephan et al.*, 2012], which we briefly summarize in the following.

The band depths (*BD*s) of the individual H_2O-ice absorptions at 1.5 and 2µm were found to be a good indicator for the relative abundance of H_2O-ice. Although, the depths of these absorptions are also influenced by the size of the H_2O-ice particles, this effect is mostly masked by the varying abundance of H_2O-ice when an additional absorbing compound like the dark material on Dione and Rhea is mixed with the H_2O ice [*Stephan*, 2006; *Stephan et al.*, 2009; *Stephan et al.*, 2010; *Stephan et al.*, 2012].

The *BD*s of the absorptions at 1.04 and 1.25µm are rather dominated by the size of the ice particles [*McCord et al.*, 1999]. The *BD*s of all absorptions were measured according to *Clark et al.* [2003]. A good approximation of changes in the sizes of the ice particles without

extensive spectral modeling can be achieved by comparing the band depth ratios (*BDR*s) of the H_2O-ice absorptions measured across Tethys to model spectra of H_2O ice [*Stephan*, 2006; *Stephan et al.*, 2011; *Stephan et al.*, 2009]. Although, the depths of the individual H_2O-ice bands are influenced by the abundance as well as the size of the H_2O-ice particles, only the particle size appears to affect the ratio of the *BD*s of two of the H_2O-ice absorptions. This assumption is valid for all incompletely saturated H_2O-ice absorptions and in case of a non-ice, visually dark contaminant, which is spectrally neutral in the near-infrared wavelength range. Since Tethys exhibits a high geometric albedo in visible light [*Verbiscer et al.*, 2007] only small amounts of a dark contaminant are expected on the satellite's surface. No absorptions exclusively associated to the dark non-ice material could be detected in the near-infrared spectral range so far [*Clark et al.*, 2008; *Emery et al.*, 2005; *Stephan et al.*, 2010; *Stephan et al.*, 2012]. Changes in the physical properties of H_2O ice, like the sizes of the individual particles are of special interest, because they are very sensitive to surface ages and weathering effects [*Stephan et al.*, 2009; *Stephan et al.*, 2012]. The *BDR* values derived from the VIMS data have been compared to *BDR* values of model spectra calculated based on the algorithm published by *Hansen* [2009] and the optical constants offered by *Grundy and Schmitt* [1998] for a surface temperature of 80K. Model spectra of H_2O ice based on the algorithm of *Hansen* [2009] were already successfully used in previous works [*Hansen and McCord*, 2004; *Hansen et al.*, 2012; *Jaumann et al.*, 2008]. Since the *BDR* values were not yet calculated in detail before for Dione and Rhea, they have been also calculated for the VIMS data presented in [*Stephan et al.*, 2010]; *Stephan et al.* [2012] and included in this work in order to compare the resulting *BDR* maps to the *BDR* map of Tethys.

In addition fresh H_2O-ice not covered yet by submicron particles show a distinct Fresnel reflection peak at 3.1µm, which also changes its shape depending on the crystallinity of H_2O ice [*Hansen and McCord*, 2004]. The crystallinity of H_2O ice is also expected to influence the wavelength positions of the H_2O-ice absorptions, in particular in case of the absorption at

2µm, shifting the band to longer wavelengths when the H_2O-ice transforms from amorphous to crystalline H_2O ice [*Clark et al.*, 2012].

It is well known that H_2O-ice is completely transparent at 0.5µm without any significant absorption by the H_2O-ice [*Dozier*, 1989]. Therefore, the geometric albedo at 0.5µm is a good indicator of how the abundance of H_2O-ice varies across Tethys' surface. We performed a photometric correction of the VIMS channel at 0.5µm using the function algorithm that the Cassini ISS team [*Porco et al.*, 2004; *Roatsch et al.*, 2009] applied to their Clear/Green-filter images, which shows Tethys as seen at a wavelength of about 0.568µm. Finally, spectral slopes [*Filacchione et al.*, 2010; *Filacchione et al.*, 2012; *Filacchione et al.*, 2007] like the slope from the visible spectral range into the ultraviolet spectral range (VIS/UV ratio: $I/F_{0.5\mu m}/I/F_{0.35\mu m}$) changes with increasing contribution of dark non-ice material, as identified on Dione and Rhea [*Clark et al.*, 2008; *Stephan et al.*, 2010; *Stephan et al.*, 2012] but has also been shown to visualize regions on the satellite's surface which have endured enhanced space weathering effects, i.e. impacting dust and particles from Saturn's magnetosphere and E Ring [*Schenk et al.*, 2011; *Stephan et al.*, 2012].

3 Overview of Tethys' geological units

3.1 The pre-Cassini view of the geology of Tethys

Voyager images of Tethys, taken in the flybys in November 1980 (Voyager-1) and August 1981 (Voyager-2), revealed a generally densely cratered landscape and two major landmarks: the graben system of Ithaca Chasma and the 400-km large impact structure Odysseus. Voyager-2 returned images with the highest resolution primarily of the Saturn-facing hemisphere. The southern latitudes of the leading and trailing hemispheres as well as the south polar terrain could not be imaged by Voyager at sufficient resolution. Voyager-based

geology of Tethys was described by *Smith et al.* [1981], *Smith et al.* [1982], and *Moore and Ahern* [1983] and is briefly reviewed here.

The densely cratered terrain shows little variation at Voyager resolution and was mapped as a more or less global unit. Most of the cratered terrain is hilly and rugged with a large number of highly degraded craters [*Moore and Ahern*, 1983; *Smith et al.*, 1982]. Odysseus is the largest, basin-sized impact feature 445 km across. Voyager frames show a rim consisting mostly of arcuate scarps, partly double, a central peak complex, and radial crater chains reminiscent of secondary craters. Distinct continuous ejecta could not be discerned.

Approximately antipodal to Odysseus, a variety of smoother, less densely cratered plains occurs near the large impact structure Penelope. *Moore and Ahern* [1983] interpreted these plains to have formed from a resurfacing event which could have been linked to the formation of Odysseus. Unlike the rugged or „weird" terrain which occurs on, e.g., Mercury antipodal to the major basin Caloris [*Neukum et al.*, 2001], however, Tethys does not show such terrain. The smooth plains at this locale were interpreted to have been resurfaced by material forming the smooth plains [*Moore and Ahern*, 1983].

Troughs, scarps and lineaments of Ithaca Chasma span approximately 270˚ around the satellite [*Smith et al.*, 1982]. This tectonic structure is up to 100 km wide and has been shown to be several kilometers deep, inferred from shadow lengths [*Smith et al.*, 1981; *Smith et al.*, 1982]. The morphologically most pronounced part of the structure is located at 0˚ W and trends approximately north-south.

Voyager images show two remarkable albedo and color features. The first one described is a longitudinal dark strip centered at 270° W with an approximate North-South trend. This feature is about 15% lower in albedo and redder with a lower violet/orange ratio than the surrounding terrain [*Buratti et al.*, 1990; *Smith et al.*, 1981]. The second feature is an elliptical

equatorial band in the leading hemisphere which is darker and bluer (higher violet/orange ratio) than the surroundings [*Buratti et al.*, 1990; *Schenk et al.*, 2011; *Stooke*, 1989; 2002]; the feature is depicted but not explicitly described by *Smith et al.* [1981] and *Smith et al.* [1982] in their preliminary albedo and topography maps.

3.2 Description of the mapped geological units

As described in our previous papers [*Stephan et al.*, 2010; *Stephan et al.*, 2012], geologic units are treated as material units rather than terrain types that (a) were formed by a specific process, or (b) were significantly resurfaced by one or even more processes. Surface morphology, therefore, is an important category to subdivide geologic units, in addition to albedo (or color) as the primary category to discriminate geologic units [*Wilhelms*, 1990]. Based on these criteria, we identified the following sets of units: (1) cratered plains materials and (2) impact-related materials, including craters and basins.

Also following the procedure in *Stephan et al.* [2010] and *Stephan et al.* [2012], craters and basins are classified by their erosional state into at least three units, a technique that has been widely used for geologic maps published by the U. S. Geological Survey [*Hansen et al.*, 2012; *Wilhelms*, 1990]. This procedure is described below in more detail.

Although crater counts were not explicitly carried out for this work, crater size distributions were measured on Tethys by some of us and have been published elsewhere [*Giese et al.*, 2007; *Wagner et al.*, 2013a; *Wagner et al.*, 2013b]. For stratigraphic purposes, we will use and discuss these results in this paper. Absolute cratering model ages for geologic units, when cited here, are derived from two cratering chronologies, (a) a chronology model with a more or less lunar-like time-dependence of the cratering rate [*Neukum et al.*, 2006; *Plescia and Boyce*, 1985], and (b) a chronology with a constant cratering rate [*Zahnle et al.*, 2003]. For a

detailed discussion of these models the reader is deferred to *Dones et al.* [2009]. The final geological map is presented in Figure 2. In the following the mapped geological units will be described in detail.

[Figure 2]

3.2.1 Cratered plains materials

a) Densely cratered plains

The most abundant geologic unit on Tethys are ***densely cratered plains (dcp)*** whose general characteristics could be defined from Voyager images [*Moore and Ahern*, 1983; *Smith et al.*, 1981; *Smith et al.*, 1982]. Here, this unit has been designated as *dcp* and represents a group in a lithostratigraphic sense [*Wilhelms*, 1990]. A typical locality is seen east of the basin Penelope, in the quadrangles *Ste-9 Penelope* and *Ste-10 Salmoneus* of the Tethys atlas [*Roatsch et al.*, 2009], which is shown in Figure 3. The unit is gently hilly, undulating, in parts rugged, and generally densely cratered. The hilly appearance results from numerous degraded impact features. The largest of the impact craters could already be discerned in Voyager data [*Moore and Ahern*, 1983; *Smith et al.*, 1981; *Smith et al.*, 1982]. Some of these degraded features are members of crater groups, but the high degradation state does not allow us to exactly define the number of craters in these groups.

Cassini ISS data covering regions not very well imaged by Voyager complete a global survey of impact basins on the order of 100 km and larger in diameter in unit *dcp*. Remarkably, these large impact features, except Odysseus, are concentrated on the trailing hemisphere in the regions south of the equator. In addition, higher-resolution ISS images show smaller, fresher

and therefore younger craters. As has been observed on Enceladus and Dione [*R Wagner et al.*, 2012], pairs or clusters of craters at all diameters and degradation states are similarly common on Tethys.

Fine-scale tectonic features are a characteristic of unit *dcp*, which is revealed only at higher Cassini ISS resolution. In the local east of the basin Penelope (Fig. 3), subparallel, narrow, comparatively fresh fractures (white arrows) cut an older set of more degraded and wider troughs, but in turn are superimposed by fresher craters up to ~ 10 km in diameter. In other localities of unit *dcp*, these narrow fractures as well as wider troughs resemble chains of circular or elliptical pits instead and probably are of impact rather than tectonic origin. The geologic boundaries of unit *dcp* are clear-cut with respect to all impact crater forms and to tectonically resurfaced units. However, boundaries between unit *dcp* and other cratered plains materials are difficult to define in some parts, as described in the following.

[Figure 3]

b) Smooth cratered plains

A less rugged, smoother but still densely cratered variety of the cratered plains is located between Ithaca Chasma and the basin Penelope, centered approximately at the trailing hemisphere. This variety was described for the first time by *Smith et al.* [1982] after the Voyager 2 encounter with Saturn and termed *plains terrain* by *Moore and Ahern* [1983]. *Smith et al.* [1982] report a lower crater frequency compared to the more rugged and hilly densely cratered plains *dcp*. Furthermore, the spatial extent of this unit was not revealed in Voyager images due to incomplete coverage (see, e.g., the geologic sketch map in *Moore and Ahern* [1983]).

In this work, we termed this unit ***smooth cratered plains (scp)***. As with unit *dcp*, the smooth cratered plains *scp* represent a rock-stratigraphic group. Despite the much higher resolution of Cassini ISS images, the boundary between unit *dcp* and *scp* is not sharp but appears to be gradational over a few kilometers or even tens of kilometers, as described by *Moore and Ahern* [1983]. On lower resolution images, the boundary is easier to locate and can be transferred to a higher-resolution map by the largest craters along its path. An example of a low-resolution ISS NAC frame, obtained in orbit 069TE, is shown in Figure 4a.

The gradational boundary between the two units *dcp* and *scp*, and the characteristics of unit *scp*, are shown at higher resolution in Figure 4b. Five large craters several tens of kilometers in diameter are located within *scp*: Phemius, Polyphemus, Icarius, Ajax, and an unnamed crater between Icarius and Polyphemus. The intercrater plains in *scp*, also between smaller craters, are comparably smooth but the transition to the hilly, rugged densely cratered plains *dcp* is clearly gradational and lacks a sharp distinct contact. Penelope, a basin of type b_2 (unit description see section 3.2.3) superimposes the boundary between the two units. We could not identify a scarp between *dcp* and *scp*, as inferred by *Moore and Ahern* [1983], but southeast of crater Ajax the boundary between the two units seems to be enhanced by a very subdued rim. The impression of a scarp in some parts could be an artifact resulting from numerous overlapping crater rims in the hilly terrain of unit *dcp* which are little discernable due to the lower-resolution Voyager images.

A color asymmetry at the trailing hemisphere, characterized by a high IR/UV ratio, coincides more or less with the smooth cratered plains *scp* but seems to be more extended than this unit. This color feature has been described by *Schenk et al.* [2011]. In Figure 4c, a color ratio of the trailing hemisphere is shown, including the boundary between *dcp* and *scp* with a dotted line. The boundary between high IR/UV albedo and the surrounding terrain with lower IR/UV

appears even less distinct than the *dcp/scp* boundary, somehow fading into the lower IR/UV terrain.

[Figure 4]

c) Lightly cratered plains

A specific variety of cratered plains found in only one location was not distinguishable at Voyager resolution. This variety is less densely cratered at medium and small crater sizes compared to units *dcp* or *scp*. We mapped and termed this unit as ***lightly cratered plains***, designated *lcp*. Its exact characterization, as well as mapping its spatial extent, is problematical, however.

The type locality south of Odysseus of unit *lcp* is shown in Figure 5. The boundary of this unit with respect to the densely cratered plains (*dcp*) is very sharp and well defined by an abrupt change in crater frequency from *dcp* to *lcp*. The unit is characterized by a rolling, undulating topography with heavily degraded craters several tens of kilometers across. Furthermore, the unit appears depleted in crater frequency at craters smaller than ~ 20 km. The sharp boundary is approximately linear (seen in an equidistant map projection used for the geologic map in Fig. 2) with more or less rectangular changes in direction reminiscent of a segmented fault.

Except in the area south of Odysseus, the boundary of this unit is difficult to identify and to locate. This is due to the fact that the region between Odysseus, Ithaca Chasma and the 100-km large crater Anticleia (whose location is shown in Fig. 6) was imaged at varying viewing conditions, sun elevations and spatial resolutions, as it is documented in the DLR ISS basemap [*Roatsch et al.*, 2009] and in color mosaics [*Schenk et al.*, 2011]. Towards the south pole, imaging at more or less constant viewing conditions and spatial resolutions is also not

complete. Therefore, mapping of unit *lcp* between Odysseus, Melanthius in the south, Ithaca Chasma in the east, and Anticleia in the north has to be regarded as preliminary. Additional images at 200 to 300 m/pxl spatial resolution taken at medium sun elevation as well as more stereo coverage is required to exactly map and characterize the spatial abundance of unit *lcp*.

The *dcp/lcp* boundary south of Odysseus is in parts marked by a topographic ridge, possibly an outer ring linked to the formation of Odysseus. This is described and shown in more detail in section 3.2.3.

[Figure 5]

d) Fractured cratered plains

The graben system Ithaca Chasma is a major landmark on Tethys and was first seen in the Voyager 1 encounter images [*Smith et al.*, 1981]. The structure is described as a branching trough featuring terraces more than 1000 km long and 50 to 100 km wide [*Giese et al.*, 2007; *Moore and Ahern*, 1983]. Ithaca Chasma follows a great circle, predominantly trends NNE-SSW and is approximately centered at the sub-Saturnian hemisphere, transgressing the equator near a longitude of 0° W. Southward, it nearly extends to the south pole. Northward, the troughs are superimposed by the, with a diameter of 92 km, relatively large crater Telemachus (53.5°N/339°W). The major part of the Ithaca Chasma structure on the sub-Saturnian hemisphere is shown in the global ISS map of Figure 2. Here, Ithaca Chasma is approximately 100 km wide and branches into two narrower, ~ 50 km wide troughs southward of 10° S. [*Giese et al.*, 2007].

We identified and mapped two facies of this unit. The first one, ***fractured cratered plains 1 (fcp_1)***, is the most common type and consists of a major terraced trough featuring numerous sub-parallel interior minor scarps and troughs. The type locality of fcp_1 south of the large crater Telemachus is depicted in Figure 6. In a digital elevation model (DEM) derived by *Giese et al.* [2007], the bounding troughs are topographically up to 6 km high with respect to the densely cratered plains *dcp* outside Ithaca Chasma which the authors attributed to flexural uplift. The depth of Ithaca Chasma was found to be on the order of 2 – 3 km, based on this DEM.

Ithaca Chasma may have been caused by expansion of internal liquid water as it froze into ice after the surface had already frozen. An alternate theory is that the impact that created the Odysseus Crater also generated forces that created Ithaca Chasma, especially since the chasm is on the opposite side of Tethys from the Odysseus Crater. The chasm and surrounding area are heavily cratered, indicating that it was formed long ago.

Results from crater counts discussed by *Giese et al.* [2007] infer that Ithaca Chasma is younger than the densely cratered plains but older than the basin Odysseus, rejecting a possible link between its formation and the Odysseus impact as has been suggested by some authors [*Moore and Ahern*, 1983]. Higher-resolution images, as those shown in detail in Figure 6, strongly imply the comparably great age of Ithaca Chasma, documented in the majority of craters within Ithaca Chasma superimposing the tectonic structures [*Wagner et al.*, 2013a; *Wagner et al.*, 2013b]. Furthermore, crater counts performed in these higher-resolution data confirm this stratigraphic finding, as well as previous results by *Giese et al.* [2007], *Wagner et al.* [2013a] and *Wagner et al.* [2013b] (see section 5).

A second facies was mapped as ***fractured cratered plains 2 (fcp_2)*** northeast of Telemachus where the Ithaca Chasma structure approximately trends west-east. In this part, the trough and the scarps are much more degraded and seem to “fade into” tectonically unmodified densely

cratered plains *dcp*. The difference in the state of degradation is clearly visible; therefore a separation between the two facies is justified.

[Figure 6]

3.2.2 Crater materials

The three erosional classes of craters c_1, c_2, and c_3 roughly represent an overlapping age sequence, meaning that c_1 craters are generally, but not necessarily older than c_2 craters (same for c_2 versus c_3 craters) [*Hansen et al.*, 2012]. No overlap in time exists for c_3 versus c_1 craters, however. In terms of lithostratigraphy, crater materials can be considered as a supergroup, with the individual erosional classes c_1, c_2, c_3 representing a rock-stratigraphic group each [*Wilhelms*, 1990]. The same subdivision for crater materials was used in *Stephan et al.* [2010] and *Stephan et al.* [2012].

a) Heavily degraded crater materials

A great number of craters on Tethys are characterized by a high state of degradation. This type is termed ***heavily degraded crater materials***, designated $\boldsymbol{c_1}$. Type examples are shown in Figure 7a. Rims of these craters are mostly degraded. In some craters, only crater ruins with ring arcs are visible (mapped with dotted lines in the global geological map in Fig. 2). No ejecta are visible. Central peaks are generally absent. Numerous smaller craters superimpose the floors of craters of type c_1. In some parts, groups of heavily degraded craters occur.

b) Partly degraded crater materials

Another rather common type of impact features are ***partly degraded craters materials***, designated ***c_2***. Type example is crater *Euanthes* (33 km diameter, 7.9° N/ 238.9° W) north of Penelope (Fig. 7b). Rims in this type are preserved but may show some degradation. Like in type c_1, central peaks are mostly absent, except in larger craters (e.g, Ajax, see Fig. 7b). Continuous ejecta are generally obliterated by superimposed smaller craters. Larger examples of c_2-craters, such as Euanthes, do have remnants of continuous ejecta, however. As type c_1, craters of type c_2 also occur in clusters or groups.

c) Fresh crater materials

A comparably small number of craters, especially at larger diameters (> 10-20 km) are mapped as ***fresh crater materials***, designated ***c_3***. These craters have pristine rims, well-developed continuous ejecta and generally central peaks. The floors and continuous ejecta display a low frequency of superimposed smaller craters indicating the relative young age of c_3-craters. Type example is *Telemachus* (92 km diameter, 54° N/ 339° W) shown in Figure 7c. Another type example is crater *Icarius* (54.5 km diameter, 6° S/ 306° W; Fig. 4b). At the given resolution 1 km/pixel of the geologic map (Fig. 2), these two craters are the only two larger features included in the map, plus a comparably small crater near Penelope with a strong H_2O ice signature (see section 4). At higher resolution, more craters of type c_3 are discernible.

From crater counts carried out on floor and continuous ejecta of Telemachus, cratering model ages of 3.6 ± 0.1 Ga (model by *Neukum et al.* [2006]), 0.74 Ga (Case A; uncertainties: 2.3 Ga (high), 0.2 Ga (low)), and 0.12 Ga (Case B; uncertainties: 0.46 Ga (high), 0.03 Ga (low)) (model by [*Zahnle et al.*, 2003]) were derived (see section 6).

[Figure 7]

3.2.3 Basin materials

An ***impact basin*** is a large impact feature that generally forms early in the history of a planet or satellite by the impact of a massive body [*Spudis*, 1993]. The boundary diameter separating craters from basins is set approximately at 300 km on the Earth's moon, and such large impact structures are characterized by (a) a complex morphology, (b) extensive ejecta blankets including secondary crater chains and radial sculptures, and (c) may display several concentric rings of ridges, scarps or graben, therefore are designated as *multi-ring basins* [*Spudis*, 1993].

Large impact structures are also abundant on the icy satellites of Saturn but lack a distinct multi-ring morphology. At least two rings, however, may be common, especially in basins on Iapetus on which most of these large impact features were observed to occur [*Giese et al.*, 2008; *Jaumann et al.*, 2009]. Unlike the rocky silicate surfaces of the terrestrial planets, complex crater morphologies and ring structures on icy satellites can be distinguished in impact features smaller than ~300 km but larger than ~100 km, especially on the Galilean satellites of Jupiter [*Stephan et al.*, 2013]. Therefore, we set the boundary between craters and basins on icy moons at a threshold of 100 – 150 km to separate basin from crater units. On Tethys, only seven impact structures significantly larger than 100 km are found. Like the crater units, these six features are classified according to their erosional state, and are designated as b_1, b_2, b_3, from older to younger.

In general, impact basins, as shown in detailed geologic maps, are characterized by a set of material units. Especially in those cases where several units can be discerned within a basin at

the map scale of 1 km/pixel, we follow the convention established for geologic mapping of the moon to consider each set of deposits associated with a specific basin as a named or unnamed group in a rock-stratigraphic sense, with each individual unit in the basin representing a formation, in turn named or unnamed [*Spudis*, 1993; *Wilhelms*, 1990].

Each basin and its associated units – similarly a major crater – provides a stratigraphic datum to be selected as a time-stratigraphic base for a subdivision of the geologic history of a body into *systems* and *series* [*Wilhelms*, 1990]. A suggestion for Tethys' time-stratigraphic column and a sequence of geologic events is presented in Figure 2 and discussed in section 5.

a) Heavily degraded impact basin materials

Three of the seven basins on Tethys can be classified as ***heavily degraded basin materials***, designated $\boldsymbol{b_1}$. These are characterized by remnants of the basin rim, which may be incomplete, and by remnants of central peak structures. These basins are *Demodocus* (125 km diameter, 59.4° S/ 18.2°W), *Dolius* (190 km diameter, 30.2° S/ 210.3°W), and *Telemus* (320 km diameter, 34.5° S/ 356.9° W). Telemus und Dolius are shown in Figure 8a and b.

The rim of Telemus, as well as that of Demodocus, is cut by the tectonic structures of Ithaca Chasma. Dolius still shows a complete but heavily degraded crater rim and an upbowed basin floor with the remnant of a central peak. At low sun, rim and central peak appear enhanced giving the impression Dolius is much fresher. In images with higher sun, however, the high state of degradation of Dolius is clearly visible justifying its classification as a heavily degraded feature.

b) Partly degraded impact basin materials

Impact features classified as ***partly degraded basin materials***, ***b_2***, have a pronounced but partly degraded rim and a steep inner scarp. No continuous ejecta are discernible. The superimposed crater frequency can be comparably high as in the surrounding cratered plains. Type locality of unit b_2 is basin *Penelope* (207.5 km diameter, 10.8° S/ 249.2° W), shown in Figure 8c. Bright fresh ice is exposed at the western interior wall. The eastern rim and interior wall appear much more degraded than the western wall. At higher resolution, fractures are seen to transect the basin, and mass wasting features can be distinguished [*Wagner et al.*, 2013a; *Wagner et al.*, 2013b]. Apart from Penelope, basin *Melanthius* (250 km diameter, 58.5° W/ 192.6° W) is the only other basin of unit type b_2.

Anaglyph images of Penelope (Fig. 9) clearly show a significantly deeper interior compared to the surrounding cratered plains, mostly likely due to little relaxation. The anaglyphs also reveal remnants of an inner ring approximately 50 km in diameter [*Wagner et al.*, 2013a; *Wagner et al.*, 2013b]. The northern and southeastern arc of this inner ring is best preserved. In both anaglyphs, the location of a landslide at the interior wall is indicated by a long white arrow. Short white arrows mark fractures cutting through the rim. Another tectonic feature, possibly a fault, transects the basin floor but seems to be absent outside Penelope (black arrows in left anaglyph).

[Figure 8]

[Figure 9]

c) Fresh basin material

The youngest basin unit, ***fresh basin material***, b_3, only has one representative on Tethys. This basin, *Odysseus*, 445 km in diameter and located at 32.8° N and 128.9° W was discovered in the first Voyager flyby (Smith et al., 1981). In Figure 8d it is shown in comparison with the other basin units. Odysseus' diameter represents almost two-fifths of Tethys itself. Usually such an impact could have shattered a solid body suggesting that the internal composition of Tethys was still partially molten at the time of the impact event. The crater's rim and central peak have largely collapsed, leaving a shallow crater, and this also suggests a terrain that was elastic enough to change shape. The subdued features of Odysseus are in contrast to many steep cliffs elsewhere. This again suggests that the ancient terrain that was still elastic enough to change shape. Even at a map scale of 1 km/pixel, several units associated with this basin can be identified. In detail, these units described below are shown in Figure 10. These units can be considered as rock-stratigraphic formations of the Odysseus group.

Basin rim and continuous ejecta

Images of the Odysseus basin at spatial resolutions of ~ 500 – 700 m/pixel show a pronounced undulating rim (Fig. 10). The rim is mostly fresh and sharp except in the eastern and southern part of the basin where it appears slightly degraded, as seen in the stereo anaglyph (Fig. 10, top right). Outside the basin rim, no clear-cut continuous ejecta blanket can be discerned (Fig. 10, detail 1 and 2).

Terrace material

Odysseus features a terraced interior (Fig. 10, detail 1 and 2) which was mapped as terrace material (*bot*). The terraces form gentle to steep-scarped lobes extending towards the basin center. The lobes and scarps are located approximately at a fraction of 75% of the basin rim diameter.

Floor material

At low sun under which most of the highest-resolution images (500 – 700 m/pxl) have been taken so far from Odysseus, the floor (unit *bof*) appears rough, rugged or blocky and features narrow arcuate fractures (Fig. 10, detail 1 and 2).

Central peak material

Odysseus is characterized by an elevated complex, including a central peak surrounded by a horseshoe-shaped mountain (Fig. 10, top right, and detail 1). The complex was named *Scheria Montes* [*Roatsch et al.*, 2009]. The central peak and the horseshoe-shaped feature were mapped as central peak material, *bocp*. The horseshoe-shaped mountain has a diameter of approximately 100 km.

[Figure 10]

Discontinuous ejecta materials (secondaries)

Towards the northeast, east, and southeast, chains of kilometer-sized craters radiate away from the basin rim (Fig. 10, top right, detail 3). These chains were mapped as discontinuous

ejecta materials (secondary craters), *bocs*. The chains are also distinguishable in Voyager images [*J M Moore, and Ahern, J. L.*, 1983]. Cassini images do not reveal any chains or discontinuous ejecta west of Odysseus.

Smooth deposits

Cassini images reveal several smooth, patchy areas associated with the radial crater chains. These features were mapped as smooth deposits (*bcsd*). The origin is unknown, but these features could represent patches of impact melt. The boundaries with respect to the densely cratered plains (*dcp*) are in many places not sharp.

4 Tethys' spectral properties

Although every VIMS spectrum of Tethys' surface is dominated by H_2O-ice, both global and regional/local spectral variations could be identified in the maps of the individual spectral parameters (Fig. 11 and 12). Spectral variations occur especially with respect to the *BD*s of the H_2O-ice absorptions and how the *BD*s of the individual H_2O-ice absorptions vary to each other. Due to the dominance of H_2O ice the individual absorption bands at 1.04, 1.25, 1.5 and 2µm are mostly distinct and more or less relatively deep in every VIMS spectrum of Tethys' surface confirming more or less pure H_2O ice. *BD*s vary only from 3.3±0.3 to 6.7±0.3% ($BD_{1.04\mu m}$), 5.0±0.3 to 13±0.3% ($BD_{1.25\mu m}$), 42.2±0.2 to 65.1±0.2% ($BD_{1.5\mu m}$) and 67.0±0.1 to 77.2±0.1% ($BD_{2\mu m}$) across the entire surface.

As mentioned above the geometric albedo at 0.5µm shows any existing changes in the abundance of H_2O ice without the influences of particle ice changes. Existing base maps of Tethys show only slight changes in the visible albedo. It reaches up to 0.9, corresponding to

almost pure H_2O ice [*Buratti and Veverka*, 1984]. Photometric measurements of Cassini data showed that the leading hemisphere of Tethys is about 10–15% brighter than the trailing hemisphere [*Buratti et al.*, 1990; *Buratti et al.*, 1998; *Emery et al.*, 2005]. Slight changes in the VIS/UV ratio (Fig. 12) are often correlated to the existence of additional non-ice compounds. No absorptions of surface compounds other than H_2O ice like observed on Dione and Rhea [*Stephan et al.*, 2010; *Stephan et al.*, 2012] could be identified.

Like the *BD*s of the individual absorptions, also the variations in the *BDR*s are small ($BDR_{2/1.5\mu m}$: 1.1±0.1 - 1.4±0.1; $BDR_{2/1.25\mu m}$: 7.1±0.3 - 13.4±0.3); $BDR_{1.5/1.25\mu m}$: 5.5.±0.3 - 9.4±0.3). The *BDR* combinations including the absorption at 1.04µm could not be measured on a pixel-by-pixel basis with sufficient accuracy because of the strong dominance of the $BD_{1.04\mu m}$ by noise signal. Nevertheless, in comparison to the H_2O-ice model spectra developed by *Hansen* [2009] based on optical constants derived by *Grundy and Schmitt* [1998] for a surface temperature of 80K *BDR*s measured on Tethys indicate changes in the average radius of the H_2O-ice particles between less than 1µm and 10 µm, which will be shown and discussed in the following sections.

4.1 Distribution of Tethys' spectral classes

Spectral variations occur either in relation to Tethys' geology, i.e. associated with specific geological/geomorphological surface features or geological units, or they mirror global/hemispherical differences. Based on variations in the spectral parameters across Tethys' surface that can be observed in the VIMS maps of Figure 11 and 12 six global and local regions of unique spectral properties can be distinguished, as described in detail below. The corresponding VIMS average spectra of the described regions are presented in Figure 13.

a) Geologically young impact features

The strongest H_2O-ice absorptions are associated with few small morphologically fresh impact craters or crater walls of larger impact craters like Telemachus (Fig. 11), which is similar to what has been observed on Tethys' neighboring satellites Dione and Rhea [*Stephan et al.*, 2010; *Stephan et al.*, 2012]. On Tethys, however, the frequency of fresh impact craters is quite low, corresponding to Tethys' geologically old surface (see section 3).

BDR maps do not show any hint of these fresh impact craters (Fig. 12). This is contrary to what is seen on Dione and Rhea where fresh impact craters like Creusa and Inktomi also exhibit relatively large H_2O-ice particles compared to their surroundings (Fig. 12) [*Stephan et al.*, 2010; *Stephan et al.*, 2012]. However, this might still be valid also for fresh impact craters on Tethys. Here these impact craters lie already within larger regions of relative low *BDR*s i.e. large particle sizes (discussed below) making their identification in the global *BDR* map difficult.

The smallest fresh impact crater (less than 10 km in diameter) with the "iciest" VIMS spectrum, i.e. exhibiting the strongest H_2O ice absorptions (spectrum *#1* in Fig. 13; $BD_{2\mu m}$=0.77±0.01; $BD_{1.5\mu m}$=0.60±0.01; $BD_{1.25\mu m}$=0.11±0.03; $BD_{1.04\mu m}$=0.07±0.03), is located at 16°S and 267°W close to the older and larger impact crater Penelope (16°S/267°W, Fig. 14). Although, the pixel ground resolution is very low in comparison to the corresponding ISS image, the "icy" spot in the VIMS data, which occurred in every VIMS observation of this region, could be easily associated to this small impact crater. It is characterized by the most pronounced, i.e. freshest, crater morphology (designated as *c3* in geological map of Fig. 2) compared to other impact craters in this densely cratered terrain. The corresponding *BDR* map (Fig. 14) also shows a slight decrease in the *BDR* value associated to this impact crater, which is not visible in the global *BDR* map (Fig. 12), confirming the assumptions that fresh surface material displays larger ice particle than their geologically older regions. Spectrum #1 is the

only one, where the Fresnel reflection peak at 3.1µm can be clearly identified supporting the interpretation of larger ice particles associated to this impact crater.

The VIMS spectrum of Telemachus (spectrum *#2* in Fig. 13; $BD_{2\mu m}$=0.71±0.01; $BD_{1.5\mu m}$=0.54±0.01; $BD_{1.25\mu m}$=0.07±0.03; $BD_{1.04\mu m}$=0.04±0.03) appears less icy than the described small fresh crater and appears rather similar to the VIMS spectrum of Odysseus (discussed in the next section). However, spectrum #2 includes the whole impact features including the crater floor, which is probably already covered by regolith. Only the steep crater walls still show the icy signature (Fig. 11).

[Figure 11]

[Figure 12]

[Figure 13]

[Figure 14]

b) Odysseus

Although also rich in H_2O ice (spectrum #3 in Fig. 13; $BD_{2\mu m}$=0.72±0.01; $BD_{1.5\mu m}$=0.56±0.01; $BD_{1.25\mu m}$=0.10±0.03; $BD_{1.04\mu m}$=0.05±0.03), the H_2O-ice absorption in the vicinity of the large impact structure of Odysseus (33°N/132°W) are slightly weaker than measured for the fresh impact craters but still deeper than measured for most parts of the surrounding areas (Fig. 11). Similar measurements fortify Odysseus' older geological age (see section 3). Despite the complex nature of this impact structure (Fig. 10), no significant spectral variations could be measured within Odysseus. Either Odysseus indeed exhibits uniform spectral characteristics, or any existing variations are not detectable due to the much lower pixel ground resolution of the VIMS data compared to the spatially highly resolved ISS images.

Even though, the *BD*s of individual VIMS observations incorporated in the BD map of Figure 11 sometimes appear to decrease toward the northwestern portion of the impact structure, it cannot be excluded that this effect is due viewing conditions. The coverage of Odysseus by VIMS observations is very limited. And, especially during Cassini's orbit 126, which offers a full coverage and the spatially best resolved VIMS data, this portion of Odysseus was hidden in darkness on the night side. Nevertheless, major parts of the crater are included in and/or exhibits the same *BD*s like a N/S oriented band on the leading hemisphere running from the northern to the southern polar region of the satellite, which is discussed in detail below. Interestingly, Odysseus shows also similar *BDR* values, i.e. similar H_2O-ice particle sizes not only like the N/S oriented band but also like the relatively fresh impact craters on Tethys (Fig. 12).

c) Ithaca Chasma

No exclusive spectral signature can be associated to Ithaca Chasma contrary to what has been observed in case of the tectonic surface features on the neighboring satellites Dione and Rhea. On Dione and Rhea the major tectonic structures located on their trailing hemispheres show a higher abundance [*Stephan et al.*, 2010; *Stephan et al.*, 2012] of relatively large H_2O ice particles (Fig. 12). In contrast, it is difficult to identify Ithaca Chasma in the global VIMS maps of Tethys (Fig. 11 and 12). Although it is well pronounced in the ISS data (Figure 2), it is almost not distinguishable from the neighborhood on a global scale. Ithaca Chasma was best observed by VIMS in Cassini's orbit 47. The VIMS spectrum (#4) in Figure 13, which corresponds to the portion of the Chasma located south of Telemachos (geologic unit *fcp*1 in the geological map of Fig. 2), rather implies that Ithaca Chasma belongs to the less icy, i.e. geologically older and weathered regions on Tethys' surface ($BD_{2\mu m}$=0.69±0.01; $BD_{1.5\mu m}$=0.49±0.01; $BD_{1.25\mu m}$=0.05±0.03; $BD_{1.04\mu m}$=0.03±0.03). Figure 15 shows the resulting

VIMS maps overlapped onto the DTM produced by *Giese et al.* [2007], which offers the unique possibility to investigate the spectral properties in comparison to the local topography (Fig. 16). Although changes in the spectral properties are apparent in the region with a light deepening of the H_2O-ice absorption at 1.5µm and decreasing of the *BDR* of the H_2O-ice absorptions at 2 and 1.5µm in the vicinity of the Chasma, these characteristics rather spectrally separate the region westwards of Ithaca Chasma (including the Chasma istself) from the region eastwards of the Chasma. Because of the Chasma's location around 0°W it exactly lies in the area of transition from the leading to the trailing hemisphere. Thus, spectral variabilities possibly mirror hemispherical differences, which exist independent of the Chasma, rather than spectral properties caused by geological surface processes (discussed below).

[Figure 15]

[Figure 16]

d) Oval albedo feature

Voyager images already showed an oval shaped surface feature in the equatorial region of Tethys' leading hemisphere characterized by a slightly darker visible albedo [*Stooke*, 2002]. This surface feature can also be seen in Cassini images [*Schenk et al.*, 2011] and extends in E/W direction between 20°N and 20°S almost across the entire leading hemisphere (Fig. 2). No effects can be recognized in the *BD* map of the H_2O-ice absorption at 1.25µm (Fig. 11) and the *BDR* map (Fig. 12) excluding particle size effects as the cause of this feature. On the other hand, the VIMS observations reveal a slight decrease in the $BD_{1.5\mu m}$ values in comparison to its northern and southern neighboring region and a less steep slope VIS/UV-

slope (Fig. 11) associated to the oval shaped dark albedo feature seen in the Cassini ISS map (Fig. 2). Although, this implies a contamination of the H_2O ice by an non-ice and absorbing species in this region (Fig. 11) as predicted by *Schenk et al.* [2011], no absorption feature could be identified in the corresponding VIMS spectrum (spectrum #4 in Fig. 13) that is exclusively associated with the visually dark material.

e) N-S oriented bands

As already indicated above, VIMS maps of Tethys show two N/S trending bands of a slightly more pronounced H_2O-ice signature in the central portions of Tethys' trailing and leading hemisphere, which could be neither observed on Dione nor on Rhea [*Stephan et al.*, 2010; *Stephan et al.*, 2012] (Fig. 12). These bands are apparent in both *BD* maps of Figure 11 and stretch from the northern to the southern polar region (Fig. 11). They appear narrower close to the equator and widen toward the poles. The band on the leading hemisphere, which is slightly suppressed where it is overlapped by the dark oval feature described above, extends at low latitudes from 80° to 130°W in the *BD* map of the H_2O-ice absorption at 1.5µm. In contrast, the band on the trailing hemisphere reaches from 250° to 290°W when measured close to the equator. Usually, higher *BD* values indicate a higher abundance of H_2O ice (N/S band on the leading hemisphere: $BD_{2\mu m}$=0.73±0.01; $BD_{1.5\mu m}$=0.54±0.01; $BD_{1.25\mu m}$=0.07±0.03; $BD_{1.04\mu m}$=0.05±0.03; N/S band on the trailing hemisphere: $BD_{2\mu m}$=0.72±0.01; $BD_{1.5\mu m}$=0.55±0.01; $BD_{1.25\mu m}$=0.09±0.03; $BD_{1.04\mu m}$=0.07±0.03), which corresponds to a higher visual albedo. The ISS albedo map (Fig. 2) as well as the VIS/UV slope map (Fig. 11), though, do not show any hint of these bands. The corresponding VIMS spectra (spectrum #5 and #6) only reveal a slightly more pronounced ice signature, i.e. deeper H_2O ice absorptions and a steeper slope from 0.5 to 2µm similar to the spectral signature of Odysseus (Fig. 13). An explanation could be that the changes in the *abundance* of H_2O ice are very small and that changes in the *particle size* of H_2O becomes more dominant in the VIMS signal. Indeed, in

the *BDR* maps these bands are characterized by a lower *BDR* value indicating larger H_2O-ice particles in these regions (Fig. 12). In all *BD* and *BDR* maps Odysseus is included in the N/S band on the leading hemisphere. On the contrary, Penelope, the geologically older impact basin (section 3.2.3) is excluded from the N/S band in the *BD* maps. In the *BDR* map this band appears to be rather independent of Penelope. The transition away from the band in eastern direction cuts the impact basin in N/S direction. The small fresh impact crater described above cannot be distinguished from the N/S band anymore in the global *BDR* map implying a similar particle size. These bands appear in numerous VIMS observations acquired during several Cassini flybys verifying that these effect is real and not an artefact of unusual observation conditions.

f) Hemispherical differences

Hemispherical differences in the spectral surface properties of Tethys' like the ones known from the neighboring satellites Dione and Rhea [*Stephan et al.*, 2010; *Stephan et al.*, 2012] can be only identified, when regional spectral differences, as described above, are excluded. These underlying hemispherical differences indicate that the major H_2O-ice absorptions are slightly weaker on the trailing hemisphere (spectrum #8 in Fig. 13; $BD_{2\mu m}$=0.67±0.01; $BD_{1.5\mu m}$=0.41±0.01; $BD_{1.25\mu m}$=0.05±0.03; $BD_{1.04\mu m}$=0.02±0.03). Indeed in the areas W and E of the N/S band on Tethys' trailing hemisphere show the weakest H_2O-ice absorptions measured on Tethys' surface demonstrating the lowest amount of H_2O- ice in the regions. This also indicated by a slightly lower visible albedo in these regions (Fig. 2).

In contrast both hemispheres show a similar relatively high VIS/UV ratio of about 1.35 (Fig. 11). The shapes of these regions, however, are different than the N/S bands of larger H_2O-ice particles. Thus, these two effects are not related to each other and two processes

independently working are responsible for these spectral characteristics. The variations in the VIS/UV ratio across Tethys' surface, however, are similar to have been observed by the Cassini ISS camera [*Schenk et al.*, 2011].

No clear hemispherical differences could be measured for the $BDR_{2/1.5\mu m}$ across Tethys' surface. Although, smallest *BDR* values interpreted as small H_2O-ice particles (<1µm) could be measured on the trailing hemisphere, Odysseus and the N/S oriented bands of larger H_2O-ice particles could mask any existing hemispherical differences. Although, the values of the $BDR_{2/1.5\mu m}$ measured for Dione and Rhea show a domination of their trailing hemispheres by relatively small particles (Fig. 12), the maps also show how the fresh impact craters Creusa (Dione) and Inktomi (Rhea) and their extended ejecta globally affect the *BDR* values of the leading hemispheres causing a generally larger average H_2O-ice particle size. On all three satellites the largest *BDR* values reach above the *BDR* value derived for our smallest model particle size of 1µm (see section 5) indicating particle sizes in the sub-micron range. If the correlation of the *BDR* values and the H_2O-ice particle size is still valid in the sub-micron region with larger *BDR* values indicating smaller H_2O-ice particles, Dione could exhibit the smallest H_2O-ice particles followed by Rhea and Tethys, respectively.

5 Discussion – Tethys stratigraphy and geological evolution

The geological units identified on Tethys' surface, their characteristics, the nature of their contact to neighboring geological units as well as their measured geological age enable us to reconstruct the stratigraphic relationships between the geological units and thus to shed light into the geological evolution of Tethys. The association of the spectral properties to either geological surface features on a local scale or to hemispheres on a global scale offers a unique possibility to investigate the processes responsible for the observed spectral properties and to further our understanding about the geological history as well as the space environment of the satellite.

The oldest geologic unit on Tethys are the densely cratered plains (*dcp*) which in this work were not further subdivided at the image scale of 1 km/pxl used for geologic mapping (Figure 2). This unit features numerous craters as well as basins > ~ 150 km in diameter of all degradation types. Figure 17 shows a cumulative distribution measured in a sample of unit *dcp* east of Ithaca Chasma, compared to other units [*Wagner et al.*, 2013a; *Wagner et al.*, 2013b]. Of the four geologic units depicted in this diagram, the cumulative frequency of the densely cratered plains *dcp* is highest next to that of unit fcp_1, indicating the age of the fractured cratered plains has an age comparable to that of unit *dcp*. Cratering model ages for *dcp* are on the order of > 4 Ga, more or less independent of the cratering chronology used [*Kirchoff and Schenk*, 2010; *Neukum et al.*, 2006; *Wagner et al.*, 2013a; *Wagner et al.*, 2013b; *Zahnle et al.*, 2003].

[Figure 17]

Although spectral properties indicate no unique surface composition of the *dcp*, this geological unit is included in the extended portion of Tethys's surface that shows the weakest H_2O-ice signature and very small H_2O-ice particles with radii <1µm (Fig. 12). These sub-micron sized particles are characteristic for all geologically old surfaces on Tethys, which have been exposed to weathering processes for billions of years (see below). Similar results could be measured on Dione and Rhea (Fig.12 and 19). Sub-micron sized H_2O-ice particles on Saturn's icy satellites already have been detected and discussed by *Clark et al.* [2012] supporting our results.

Impact crater and basin units *c*1, *b*1 and *b*2 date back to the formation of this oldest geologic unit, based on their high state of degradation as well as their superimposed crater frequencies,

especially on units *b*1 and *b*2. In terms of large impact structure density, Tethys is characterized by the unique fact that basins are preferentially concentrated on the southern hemisphere, except Odysseus. The number or frequency of large craters and/or basins on the other mid-sized satellites of Saturn is either too limited (e.g., Mimas, Dione) to infer a spatially preferential occurrence, or they are more or less uniformly distributed across the surface (e.g., Rhea, Iapetus) [*Giese et al.*, 2008; *Kirchoff and Schenk*, 2010; *Stephan et al.*, 2010; *Stephan et al.*, 2012]. Due to the fact that basins of type *b*1 and *b*2 are still distinct despite their high degradation state, it is apparent that they were formed preferentially on Tethys' southern hemisphere. A complete degradation of pre-existing basins on the northern hemisphere is unlikely since no significant difference in morphology and/or crater frequency between northern and southern hemisphere is detectable. Furthermore, measured crater frequencies on Tethys do not show an equilibrium distribution or saturation that could have been responsible for erasing age differences [*Schmedemann et al.*, 2014]. Spectrally, these impact craters and basins cannot be distinguished from their surroundings, which supports their high geological age (Fig. 11 and 12).

The smooth cratered plains unit *scp*, like *dcp*, is interpreted as an old unit, but has a lower crater frequency according to Smith et al. (1982). In crater counts performed by *Kirchoff and Schenk* [2010] on Tethys, no distinction was made between the densely cratered plains *dcp* and the smooth cratered plains *scp* in their measurements. Because of the antipodal location of unit *scp* with respect to the Odysseus basin, *J M Moore, and Ahern, J. L.* [1983] discussed the possibility that the formation of this major impact basin also caused the formation of the smooth plains. However, no pervasive resurfacing affecting the high density of craters in *scp* caused by the Odysseus impact event is detectable. Seismic shaking from the impact event was cited as the most likely cause for the origin of the smooth plains [*J M Moore and Schenk*, 2007], resulting in a process of "smoothing" the former rugged and hilly terrain of unit *dcp*. Other processes such as cryovolcanic resurfacing by liquid material inferred as a possible

cause for smooth terrain formation [*Schenk and Moore*, 2009] can be ruled out since the boundary between units dcp and scp is in most parts gradational. A similar high geological age supported by the fact that both units, i.e the *scp* and *dcp*, do not show any differences with respect to their spectral signature (Fig. 12 and 13). Any differences are probably masked and/or eliminated due to uppermost surface regolith as a result of billions of years of impacts and space weathering processes.

We interpret the prominent tectonic feature Ithaca Chasma, mapped in two varieties of fractured cratered plains (units fcp_1 and fcp_2) to have formed early in Tethys' geologic history. The state of degradation of the scarps and troughs and the high density of craters mainly of type c_1 and c_2 superimposing these tectonic structures in Ithaca Chasma infer a time or time period of origin prior to Odysseus. A formation as a consequence of impact deformation by the Odysseus impact event, as suggested by, e.g., *Smith et al.* [1981], seems less likely according to measured crater size frequency distributions [*Wagner et al.*, 2013a; *Wagner et al.*, 2013b]. Older, even Voyager-based measurements of the crater distribution support these results [*Giese et al.*, 2007; *Plescia and Boyce*, 1982]. It could be argued that the high density of craters superimposed on scarps and troughs of Ithaca Chasma was caused by extensive secondary cratering from the Odysseus impact event. However, this can be more or less excluded since the superimposed craters in turn show wide varieties of degradation states and therefore were formed over a prolonged period of time rather than by a single event.

Apart from a supposed impact-related origin Ithaca Chasma could have formed from two sources of stress: (1) Freeze expansion of H_2O ice [*Moore and Ahern*, 1983] or (2) tidal stress due to a high excentricity [*Chen and Nimmo*, 2008]. *Giese et al.* [2007] performed stereo analysis using Cassini ISS images in order to determine the lithospheric thickness and heat flux in Ithaca Chasma. Their results are compatible with Ithaca Chasma being an old surface feature, supporting an age from crater counts derived with lunar-like cratering chronology

models [*Neukum et al.*, 2006; *Plescia and Boyce*, 1982], which is on the order of 4.0 Ga [*Giese et al.*, 2007; *Wagner et al.*, 2013a; *Wagner et al.*, 2013b]. A younger formation age for Ithaca Chasma from the application of the constant cratering rate model by *Zahnle et al.* [2003], order of ~3 Ga, has been considered unrealistic, based on a plausible thermal history model and heat flux of Tethys [*Giese et al.*, 2007; *Multhaup and Spohn*, 2007].

On the other hand, an age younger than ~ 4 Ga could be possible if Ithaca Chasma originated from tidal stress associated with a higher eccentricity in a more recent past (more recent than ~ 4 Ga) due to a 3:2 orbital resonance with Dione [*Chen and Nimmo*, 2008]. The present-time eccentricity is close to zero and Tethys therefore is tidally inactive, despite a resonance between Tethys and Mimas and a resonance between Enceladus und Dione respectively. According to *Chen and Nimmo* [2008] it is not certain how the orbit of Tethys evolved into this present-time orbital configuration from a higher-eccentricity paleo-resonance with Dione possibly accounting for the formation of Ithaca Chasma. In a more recent work of *Zhang and Nimmo* [2012] imply that the impact of Odysseus could have broken a 3:2 Tethys-Dione paleo-resonance.

In the VIMS data, the major tectonic surface features on Dione and Rhea show a distinct H_2O-ice signature and a distinct morphology similar to fresh impact craters on these satellites pointing to a geologically younger age [*Stephan et al.*, 2010; *Stephan et al.*, 2012]. The spectral signature of Ithaca Chasma on Tethys (geologic unit *fcp*), however, is almost nonexistent anymore and is probably masked by spectral signatures of the surface caused by younger surface (exogenic) processes (discussed below). On the contrary, Odysseus, as stated above, shows a distinctly icier, i.e. fresher H_2O ice signature. Thus, our measurements support the thesis that the formations of Ithaca Chasma took place early in Tethys' history but before the Odysseus impact event happened. Therefore, both events are unrelated to each other, supporting the results of *Giese et al.* [2007].

The interpretation and definition of the stratigraphic position of the geologic unit mapped as lightly cratered plains (*lcp*) is problematic, mostly due to insufficient imaging, as described above. The boundary between this unit and unit *dcp* is linear and very sharp south of Odysseus, inferring a tectonic influence, as shown in Figures 5 and 18. The subdued morphology of most large craters as well as the low density of smaller craters (≤ 20 – 30 km in diameter) indicates a resurfacing process of so far unknown origin. The spatial extent of this unit is also unknown due to the reasons cited above. In the images available at present, Ithaca Chasma seems to about against the eastern boundary of this unit. Northward and southward, the boundaries of *lcp* with respect to other units must still be considered as preliminary. The fact that both the modified cratered plains units *scp* and *lcp* are located in proximity to Ithaca Chasma suggests that these two units, as well as the fractured cratered plains fcp_1/fcp_2 of Ithaca Chasma could have a common origin related to endogenous processes. This needs further study, based on improved ISS image coverage that might possibly become available toward the end of the Cassini mission.

Odysseus is the youngest of the Tethyan basins and was formed after the cratered plains varieties. However, the resurfacing process in unit *lcp* that erased most of the mid-sized and smaller craters could have taken place after the Odysseus impact event. Measurements of crater frequencies verify that the basin is younger than Ithaca Chasma, based on the observation that the majority of the craters superimposes the tectonic structures within Ithaca Chasma and assuming that they are primary craters and not Odysseus secondaries [*Giese et al.*, 2007; *Wagner et al.*, 2013a; *Wagner et al.*, 2013b]. Cratering model ages of Odysseus from crater counts are on the order of 3.8 Ga in the model by *Neukum et al.* [2006], versus 2.1 Ga (Case A) and 400 Ma (Case B) in the model according to *Zahnle et al.* [2003] [*Wagner et al.*, 2013a; *Wagner et al.*, 2013b].

[Figure 18]

The close proximity of obvious secondary crater chains (unit *bocs*) to the basin rim (*boc*) pointing radially away and the apparent lack of an extended continuous ejecta blanket suggests a low impact energy, possibly from a large projectile impacting at a comparably low velocity. *Zhang and Nimmo* [2012] discuss that the Odysseus projectile might have had its origin within the Saturnian system and possibly represented a small Saturnian satellite, impacting at low ~ 500 m/sec, which implies a planetocentric (Saturno-centric) impactor. The origin of the Odysseus unit designated as *bosd* is uncertain. Here it is interpreted as smooth deposits, possibly impact melt. Areas of *bosd* are spatially close to the secondary chains (*bocs*). Their boundaries are mostly indistinct. Higher-resolution images are necessary for studying these features in more detail.

Several geologically old impact basins were observed with Odysseus the only one with a significantly icier spectral signature, pointing to a younger geologic age than most parts of the surface including Ithaca Chasma. Usually, surface features formed due to excavation of subsurface material like during an impact event and tectonic activity are assumed to exhibit a similar spectral signature if the space environment (discussed below) is not much different in these locations. Interestingly, the size of the H_2O-ice particles is relatively large and similar to fresh icy material on Tethys (ice particle radius of about 5µm) and observed in case of fresh impact craters and tectonically resurfaced regions on Dione and Rhea (Fig. 19). Thus, Odysseus' spectral characteristics are interpreted to be a remnant of its primordial surface composition. On the contrary, Odysseus shows the same signature than the N/S oriented icy band, which is located together with Odysseus on Tethys leading hemisphere indicating a possibly relationship with respect to their formation. However, the N/S band cannot be associated to any surface feature and rather points to originate due to an exogenic effect.

[Figure 19]

After the formation of the cratered plains varieties including the large basins and degraded basins, the majority of impact craters were emplaced and continuously degraded by space weathering as well as micrometeorite bombardment. These craters are mostly of types (units) c1 and c2. Individually, larger craters of these types may be dated by counting smaller superimposed craters in higher-resolution ISS images in order to define their relative position in the stratigraphic column. Only the youngest craters of unit c3 show a strong correlation with H_2O ice absorption features in Cassini VIMS data as, e.g., the impact crater east of basin Penelope (Fig. 14), or Telemachus, the largest c3 crater on Tethys (Fig. 4). Telemachus was dated by crater counts. Its cratering model age is ~ 3.6 Ga according to the *Neukum et al.* [2006] model, or ~ 700 Ma (Case A) and ~ 100 Ma (Case B) according to the *Zahnle et al.* [2003] model [*Wagner et al.*, 2013a; *Wagner et al.*, 2013b]. These youngest surface features are usually characterized by clean H_2O ice of relatively large particle sizes with particle radii of about 5µm (Fig. 19). Interestingly, H_2O-ice particle sizes measured of fresh impact craters on other Saturnian satellites like Inktomi on Rhea and Creusa on Dione are similar (Fig.13 and 19). Assuming this material is freshly excavated subsurface material, the relatively large H_2O ice particles imply that the crustal material of these satellites is similarly chemically and physically composed. However, this cannot explain the particle sizes of the H_2O ice in the N/S band, which lies in the vicinity of Odysseus. This aspect is discussed below.

Weathering of the surface material due to impacting micrometeorites, dust and/or H_2O-ice particles from Saturn's magnetosphere and rings are still actively altering the chemical and physical properties of Tethys' surface material. Thus, the hemispherical differences, the E-W-

as well as N-S-trending albedo and color features in the low latitudes on the leading hemisphere and on the center of the trailing hemisphere may have formed recently, or, more likely, they have been persisting for a long (>> 1 Ga) time and are subject to a constant removal and re-deposition of material.

Differences in the strength of the H_2O-ice absorptions between the leading and trailing hemisphere on Tethys are expected to mirror the influence of the space environment on Tethys' surface properties. Subdued *BD*s of the H_2O-ice absorptions at 1.5 and 2µm due to visually dark material on the satellites' trailing hemisphere were also measured on Dione and Rhea [*Clark et al.*, 2008; *Stephan et al*., 2010; *Stephan et al*., 2012]. Dust particles in Saturn's magnetosphere are known to impact their trailing hemispheres and to cause sputtering of H_2O-ice particles, which can result in a tenuous exosphere of O_2 like detected at Rhea [*Teolis et al.*, 2010], whereas bombardment by small E-ring grains brightens the leading hemispheres.

The subdued albedo and *BD*s of the equatorial E-W trending band on Tethys' leading hemisphere corresponds to the dark bluish band observed in Cassini ISS data interpreted to be formed by irradiation of the surface by incident MeV electrons, which are expected to rotate in a direction opposite to the main plasma flow [*Schenk et al.*, 2011]. Weathered regions on Tethys, especially the anti Saturnian hemisphere, are dominated by sub-micron sized H_2O-ice particles (Fig. 19), which confirm studies by *Clark et al.* [2012] and probably results from an undisturbed deposition of micrometeorite-gardened micron to sub-micron particles [*Hansen et al.*, 2005].

On the contrary to what to expect for surface areas experiencing an enhanced bombardment, the N-S trending icy bands show unusual large ice particles similar to fresh impact craters (see above). Usually, relatively large ice particles only occur in regions that did not experience significant space weathering (either there are geologically young or are shielded from micro-meteoritic and/or radiation bombardment) [*Clark et al.*, 2008; *Stephan et al.*, 2010; *Stephan et*

al., 2012] or occur in regions of higher surface temperature [*Jaumann et al.*, 2008; *Stephan et al.*, 2009]. Neither explanation works for the N-S bands on Tethys.

Because of the similar spectral signature like Odysseus, a formation of these bands related to the Odysseus impact event cannot be ruled out. Several authors discussed the influence of the Odysseus impact event on Tethys, which might have caused a temporary non-synchronous rotation of Tethys that has now become synchronous again. No evidence of any surface signature related to an at least temporarily non-synchronous rotation like cycloid linear surface features, as observed on the Jovian satellite Europa [*Hurford et al.*, 2007], could be identified so far. *Zhang and Nimmo* [2012] only propose an ancient episode of heating and deformation on Tethys, which has been attributed to its passage through a 3:2 resonance with Dione and possibly was broken by the Odysseus impact event [*Zhang and Nimmo*, 2012].

Since these N-S trending bands occur mostly independent of geological features, they are interpreted as relatively recently formed. Tethys exhibits some thermal anomalies, with higher surface temperatures corresponding to the low-albedo feature close to the equator of Tethys' leading hemisphere [*Howett et al.*, 2012]. No thermal characteristic can be connected to the N-S bands. The location and overall shape of these bands also do not fit the areas expected to endure enhanced impacts of particles from Saturn's magnetosphere as well as from the E ring. However, Tethys orbits Saturn relatively close to the E ring as well as in a region of dense plasma of Saturn's magnetosphere, which might also cause the higher porosity of Tethys' surface compared to the other Saturnian satellites derived from UV measurements [*Royer and Hendrix*, 2014]. Thus, the interaction between the surface material and the space environment might be more complex here and different from that seen on Dione and Rhea [*Stephan et al.*, 2010; *Stephan et al.*, 2012].

6 Summary

Tethys' surface shows geological and spectral surface characteristics, whose appearance, nature and spatial distribution mirror those identified on Tethys' neighboring satellites but partly are unique in the Saturnian system. The geological units are in places associated with the spectral variations of relatively large pure H_2O ice particles in particular at fresh impact craters. The very few fresh impact craters observed on Tethys as well as Dione and Rhea exhibit similar particle sizes implying similar chemical and physical properties of the subsurface material of these satellites. Geologically old, weathered regions instead are dominated by very small submicron-sized particles.

Our geological investigations confirm that Odysseus with its pronounced morphology and ejecta cannot belong to the oldest features. It is clear that the Odysseus impact event globally affected the satellite. The results of the combined analysis of spectral and imaging data, however, contradict the theories that the Odysseus impact event caused the formation of Ithaca Chasma.

But it is not certain yet if the Odysseus impact event is connected to the formation N-S trending 'icy' bands that are consistent with Odysseus in abundance and particle size of H_2O ice. These bands cannot be correlated to expected pattern due to recent radiation effects and/or variations in surface temperature. Although, it cannot be excluded that the Odysseus impact event led to their existence, further investigations are needed to identify the processes responsible for their formation and their possible relationship to either Odysseus or the interaction of Tethys' surface material with Saturn's rings and magnetosphere.

7 Table Captions

Table 1: Tethys Tour Event Summary of non-Targeted (nT) Cassini Flybys at Tethys offering VIMS observations with pixel ground resolutions of better than 60 km/pixel sufficient for spectral and spatial analysis. Note that the distance between the spacecraft and Tethys surface and phase angle is given for the time at closet approach.

8 Figure Captions

Figure 1: Coverage of Tethys by VIMS observations summarized in Table 1 depending on: ***(a)*** pixel ground resolution and ***(b)*** phase angle.

Figure 2: Global base map of Tethys acquired by the Cassini ISS instrument and published in *Roatsch et al.* [2009] used for the geological mapping and comparison to Tethys' spectral properties ***(top)*** and the achieved geological map ***(middle)*** and stratigraphic relationships of Tethys' geological units ***(bottom)***. Names of discussed impact structures: Ajax (Aj); Antinous (An); Dolius (Do); Euanthes (Eu); Eurymachus (Ey); Icarius (Ic); Laertes (La); Melanthius (Me); Nestor (Ne); Penelope (Pe); Phemius (Ph); Polyphemus (Po); Poseidon (Ps); Telemachus (Te); Telemus (Tm). The dashed line indicates the visually dark oval shaped and EW oriented surface feature on Tethys' leading hemisphere identified first in Voyager images by *Stooke* [2002].

Figure 3: Type locality of the geologic unit *densely cratered plains* (*dcp*) east and northeast of the basin Penelope (P). The detailed view reveals the dominantly rugged and hilly morphology and topography of this unit. Fractures of two different types are indicated by arrows (white: narrow, fresh fractures; black: wider, more degraded fractures and troughs). Crosscutting suggests that the narrow fractures are younger than the wider forms. Dotted

outlines indicate ruins of heavily degraded craters not classified as crater units c_1. Crater Euanthes (E) is the freshest crater form in the depicted area and was mapped as c_2. The location of the type locality of the *dcp* is shown in the global ISS map of Tethys (Fig. 2).

Figure 4: ***(a)*** Low resolution image from orbit 069TE, ISS NAC frame N1590391036, oblique view showing the large fresh crater Telemachus (Te) and the approximately north-south trending graben system of Ithaca Chasma (IC) superimposed by Telemachus; the roughly circular boundaryh between units *dcp* and *scp* is shown as a dotted line. ***(b)*** Type locality of unit *scp*, smooth cratered plains; detail of a mosaic of ISS NAC images taken in orbit 119TE, observation sequence GEOLOG001, scale 720 m/pxl (orthographic projection at 2° N/ 247° W); impact features indicated are Penelope (Pe), Phemius (Ph), Polyphemus (Po), Icarius (Ic), Ajax (Aj), and Euanthes (Eu). ***(c)*** Color ratio of the trailing hemisphere of Tethys, obtained in orbit 119TE, observation sequence LOWPHASE001, at a scale of 1.4 km/pxl. Ratios of Cassini ISS filters IR3/UV3, IR3/GR and UV3/IR3 are set to red/green/blue respectively. The same craters as in (b) included, plus craters Antinous (An, basin-sized) and Irus (Ir). The location of the type locality of the *scp* is shown in the global ISS map of Tethys (Fig. 2).

Figure 5: Type locality of unit *lightly cratered plains* (*lcp*) and its boundary with unit *dcp* (thick arrows). Impact features indicated are the type b_2 basin Melanthius (M), Poseidon (P), Eurymachus (E), and the heavily degraded craters Nestor (N) and Laertes (L). A part of the tectonic graben in Ithaca Chasma (IC), unit fcp_1, is seen at the right. Part of a mosaic constructed from ISS NAC frames from orbit 026TE with an average resolution of 720 m/pxl. The *dcp/lcp* boundary is shown here as a curved line due to the orthographic projection but is more or less linear in cylindrical map projections as used in DLR basemap (Fig. 2). See also Figure 17 for more details.

Figure 6: Detailed image of Ithaca Chasma at higher resolution, showing the type locality of unit *fractured cratered plains (fcp1)*. Part of an ISS NAC mosaic from orbit 047TE, ISS observation GEOLOG002, map scale 120 m/pxl. Further explanation is given in text.

Figure 7: Crater material units, mapped according to their erosional state (see text for explanation). ***(a)*** heavily degraded craters materials, unit c1; some craters are ruins whose rims are barely visible (arrows; in Fig. 2 mapped with dotted lines only). ***(b)*** Partly degraded crater materials, unit c2; type locality near the basin Penelope, largest crater of this type in the area shown is Euanthes. ***(c)*** Fresh crater materials, unit c3; typical example of this class is crater Telemachus showing a very low superimposed crater frequency implying a young age.

Figure 8: Impact basin material units, mapped according to their erosional state (see text for explanation). ***(a)*** Heavily degraded basin materials, b_1; degraded rim of basin *Telemus*, indicated by white arrows; a degraded central peak is marked by a black arrow. ***(b)*** *Dolius*, type of heavily degraded basin materials, b_1, has a full rim preserved and a degraded central peak. ***(c)*** Partly degraded basin materials, b_2; type locality is *Penelope*. ***(d)*** Type locality of *fresh basin materials*, b_3 (= *bo*). The only feature representing this type is *Odysseus* and its associated units.

Figure 9: Anaglyph images of basin Penelope (type locality of unit b_2). Height exaggeration is higher in the version on the right. The anaglyphs were put together from images obtained in orbit 136TE. For the explanation for marked features see text. To view the anaglyphs, use red-blue glasses (red on left eye, blue on right).

Figure 10: Geologic units mapped in Odysseus, the only representative of basin type b_3. ***Top left***: Overview of Odysseus, rectangles indicate the location of the details shown in (1) – (3). Mosaic of NAC images from orbit 049TE (570 m/pxl scale). ***Top right:*** Stereo anaglyph of Odysseus, (orbit 049TE images). ***(1)*** Detail with units *boc* (rim and continuous ejecta), *bot*

(terraces), *bof* (floor), and a radial crater chain, possibly of secondary origin (*bocs*). ***(2)*** Part of the basin interior with units *bocp* (central peak complex), *bof* (floor material), *bot* (terraces), and *boc* (rim and continuous ejecta). ***(3)*** Area to the southeast of Odysseus with radial crater chains (*bocs*) and smooth deposits (*bosd*).

Figure 11: Global VIMS maps showing the variations in the band depth (*BD*) of the H_2O-ice absorptions centered at (top) 1.25µm and (center) at 1.5µm as well as (bottom) in the VIS/UV slope across Tethys' surface.

Figure 12: Global VIMS maps showing the variations in the band depth ratio (*BDR*) of the H_2O-ice absorptions at 2 and 1.5µm measured for (top) Tethys, (center) Dione and (bottom) Rhea. Note that the color bar is adapted separately for each satellite to show the best contrast.

Figure 13: Average VIMS spectra of spectrally different regions described in section 4, which can be distinguished in the global VIMS maps of Figure 12 and 13 (see text for description). Spectra are normalized at 2.7µm and stacked for better comparison.

Figure 14: Close up view of the unnamed small fresh impact crater located at 16°S and 267°W and the corresponding VIMS maps of the spectral parameters $BD_{1.5\mu m}$ and $BDR_{2/1.5\mu m}$.

Figure 15: Close-up view onto Ithaca Chasma – combination of VIMS data with ISS images and DTM.

Figure 16: Topographic profiles of the Ithaca Chasma region combined with VIMS results,

Figure 17: Cumulative crater size frequency diagram showing the stratigraphic sequence from old densely cratered plains (unit *dcp*), fractured cratered plains in Ithaca Chasma (unit *fcp1*), several units in basin Odysseus (sum of counted areas in units *boc*, *bof* and *bot*, labels as *ody* in the diagram), to the young crater Telemachus (unit c_3, sum of areas of measurements on floor and continuous ejecta, labeled as *tlm* in diagram).

Figure 18: Geology of the surrounding of Odysseus. ***Left***: ISS Nac frame N1481443192 (orbit 00BTE, scale 12.5 km/pxl), arrows indicate the second approximately concentric outer ring (ridge) of Odysseus. ***Middle***: Mosaic of images from sequence 049TE_MORPHO007_PRIME (orthographic projection, center at 2° S/ 120° W, map scale 570 m/pxl; highpass filtered). ***Right***: Mosaic of images from sequence 026TE_TETHYS002_VIMS (orthographic projection, center at. 40° S/ 80° W, map scale 720 m/pxl; highpass filtered). Geologic boundary between units *dcp* and *lcp* indicated, question mark were uncertain (see text). Large craters/basins: Odysseus (Od) and Melanthius (Me).

Figure 19: H_2O-ice particle radii of various terrains on Tethys (described in section 4), Dione and Rhea derived from the *BDR* values measured in the corresponding VIMS spectra (Fig. 13) and theoretical H_2O-ice model spectra of *Hansen* [2009] representing the spectral properties of H_2O ice at a temperature 80K based on the optical constants derived by *Grundy and Schmitt* [1998] .

9 Tables

Mission	Date	Cassini Flyby	Closest Approach [km]	Phase Angle [°]	Number of VIMS cubes	Pixel ground resolution [km/pixel]
Nominal	2005-03-09	4	83,000	64	17	2.5 - 52
	2005-05-02	7	52,000	110	15	31 - 40
	2006-07-23	26	120,000	29	8	29 - 63
	2006-11-09	32	212,300	37	11	49 - 59

	2007-05-26	45	102,000	78	27	26 - 69
	2007-06-27	47	16,000	116	30	5 - 25
	2008-05-10	67	187,000	72	14	44 - 91
Equinox	2008-11-24	94	24,233	159	10	13 - 22
	2009-10-14	119	85,262.7	76	14	29 - 32
	2010-02-13	126	111,962.0	114	10	41 - 43
	2010-08-14	136	36,965.5	90	88	9 - 62
Solstice	2012-04-14	164	7,632.4	123	103	7 – 85
	2012-06-28	168	68,828.2	79	24	16 - 19
	2015-04-11	214	52,863	32	57	12 - 29

Table 1

10 Figures

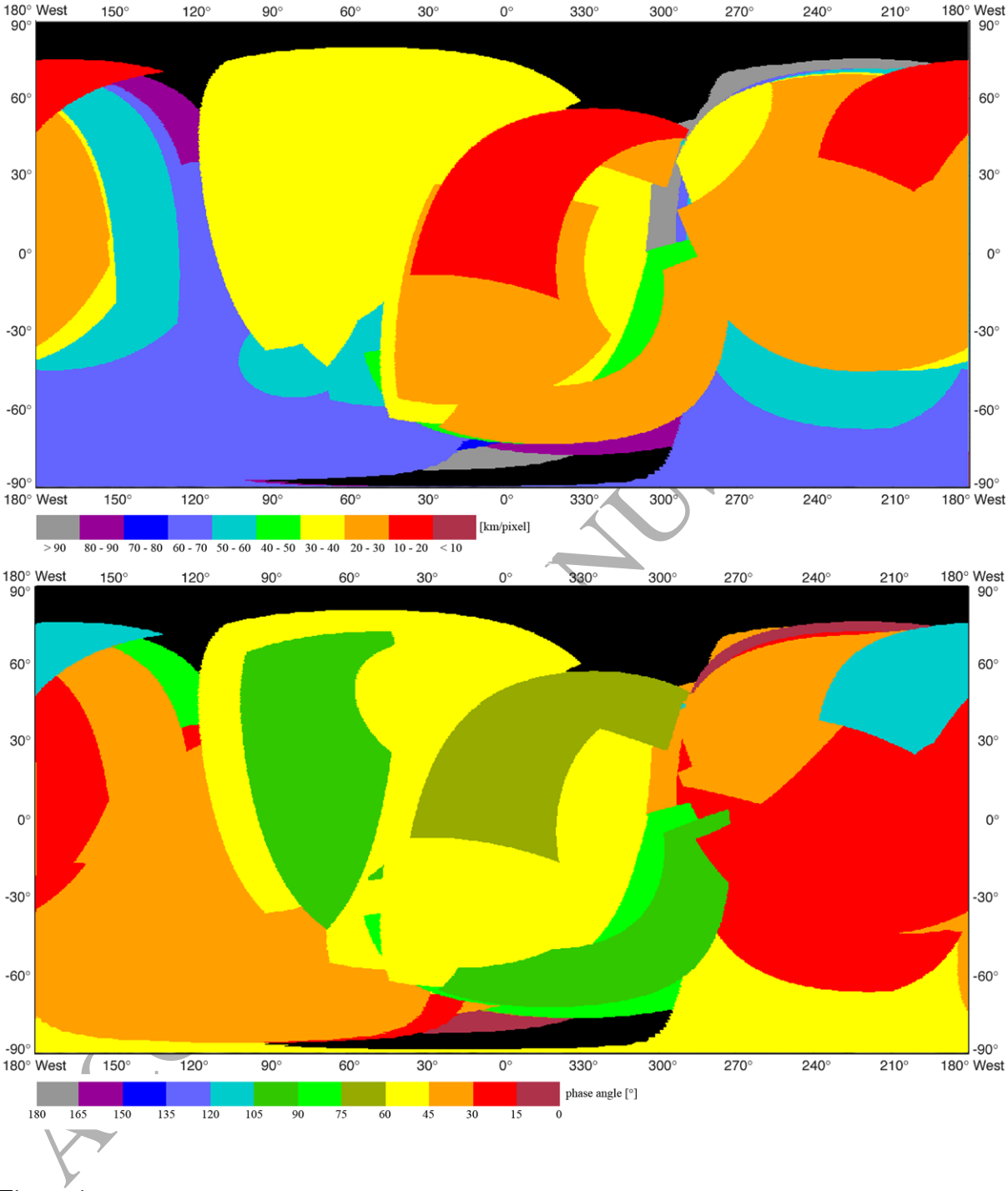

Figure 1

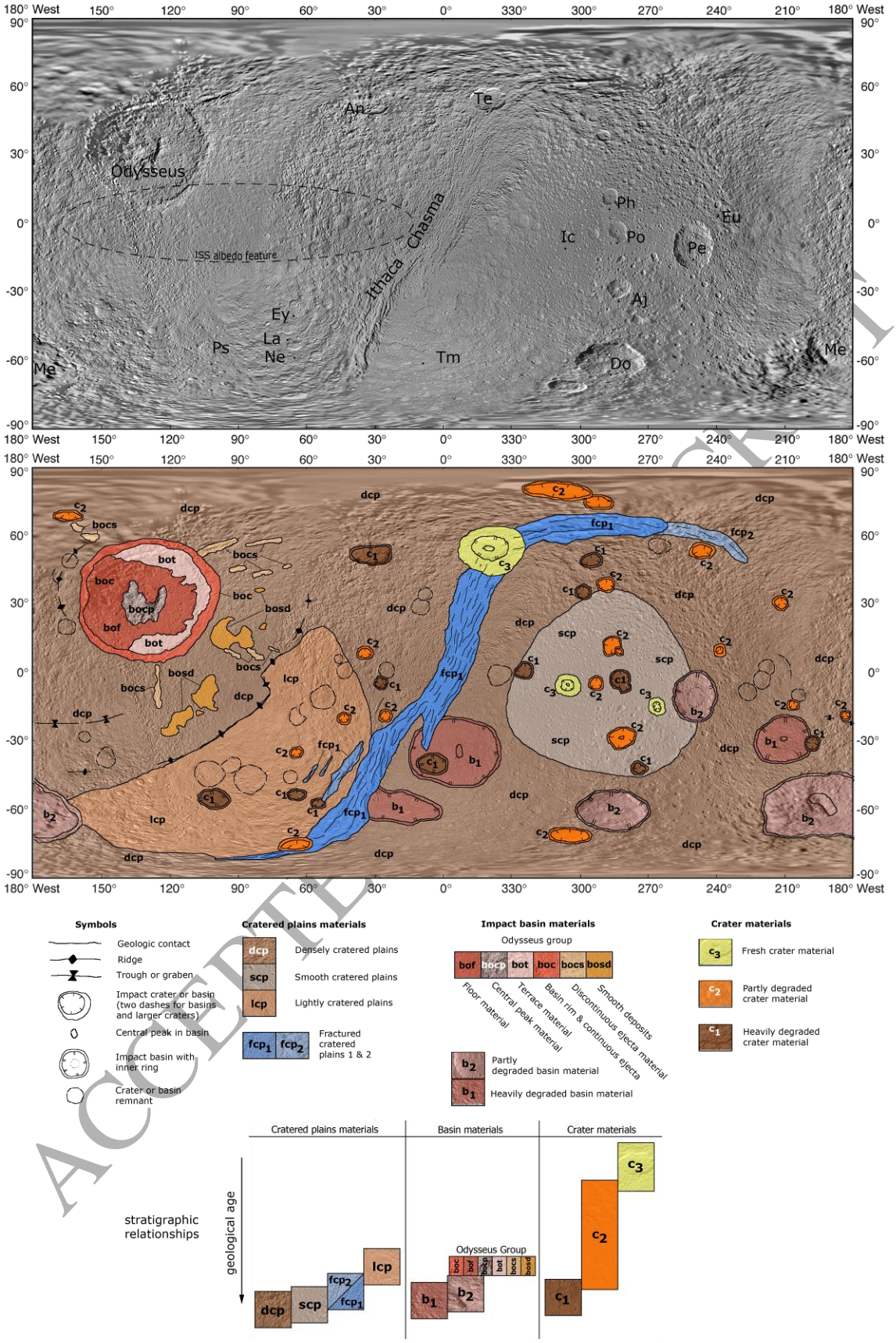
Odysseus
An
Te
Ithaca Chasma
ISS albedo feature
Ph
Eu
Ic
Po
Pe
Aj
Ey
La
Ne
Ps
Tm
Do
Me
Symbols
Geologic contact
Ridge
Trough or graben
Impact crater or basin (two dashes for basins and larger craters)
Central peak in basin
Impact basin with inner ring
Crater or basin remnant
Cratered plains materials
dcp Densely cratered plains
scp Smooth cratered plains
lcp Lightly cratered plains
fcp1 fcp2 Fractured cratered plains 1 & 2
Impact basin materials
Odysseus group
bof bocp bot boc bocs bosd
Floor material
Central peak material
Terrace material
Basin rim & continuous ejecta material
Discontinuous ejecta material
Smooth deposits
b2 Partly degraded basin material
b1 Heavily degraded basin material
Crater materials
c3 Fresh crater material
c2 Partly degraded crater material
c1 Heavily degraded crater material
Cratered plains materials
Basin materials
Crater materials
geological age
stratigraphic relationships
Odysseus Group

Figure 2

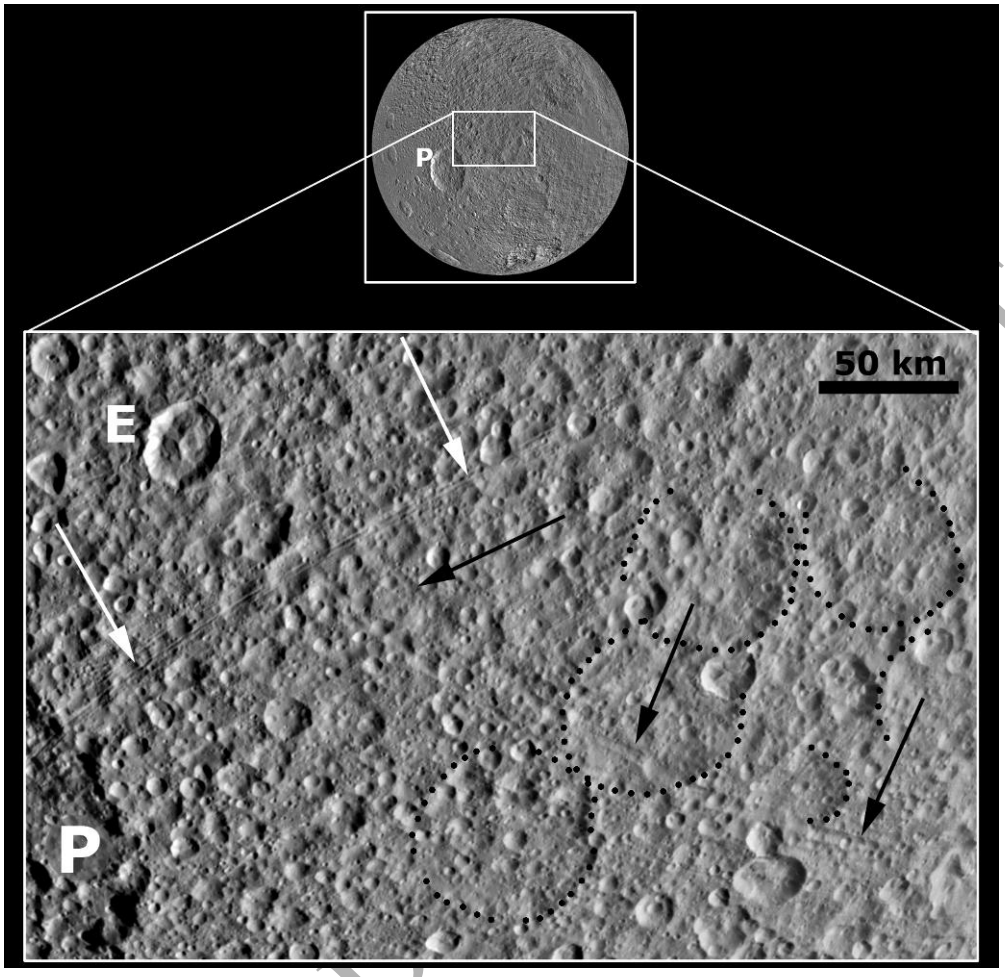

Figure 3

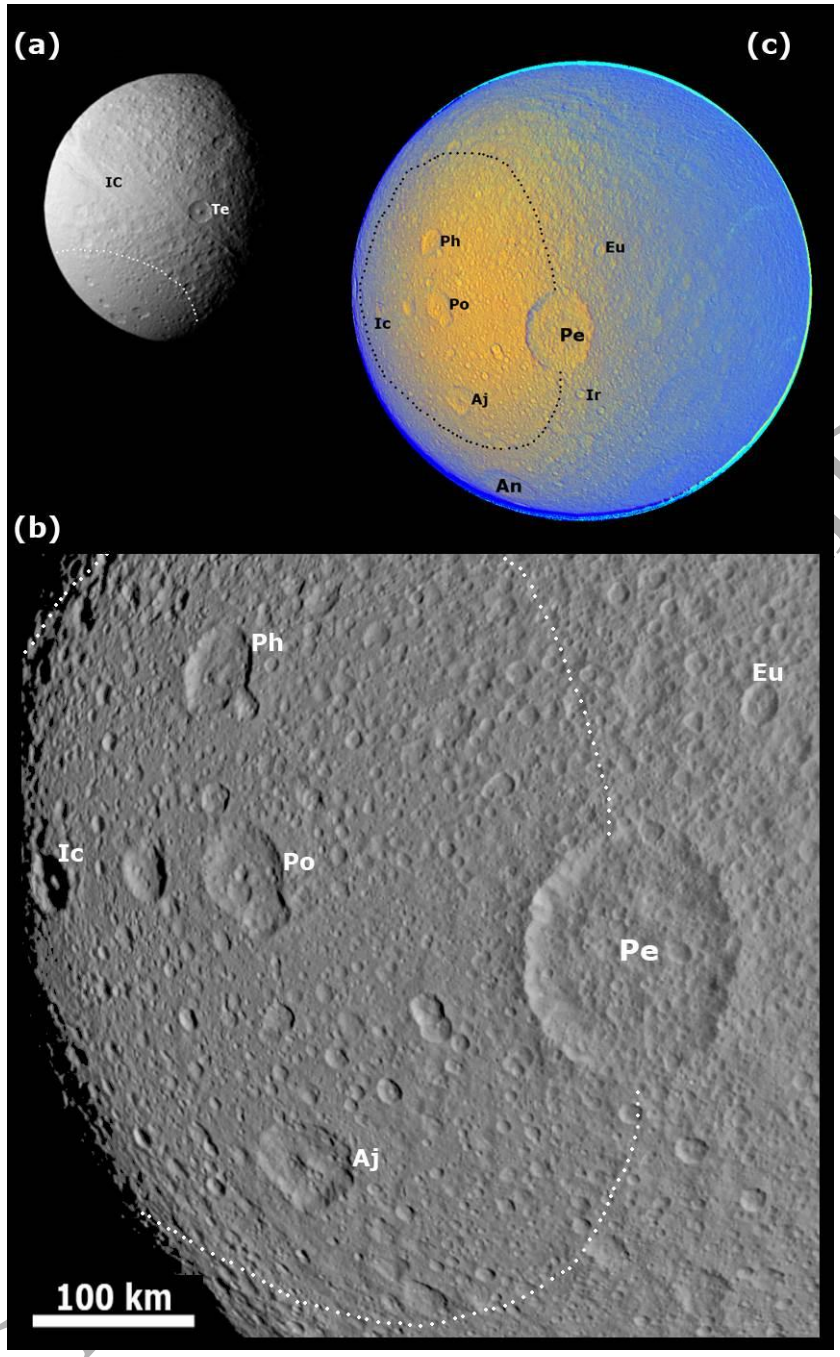

Figure 4

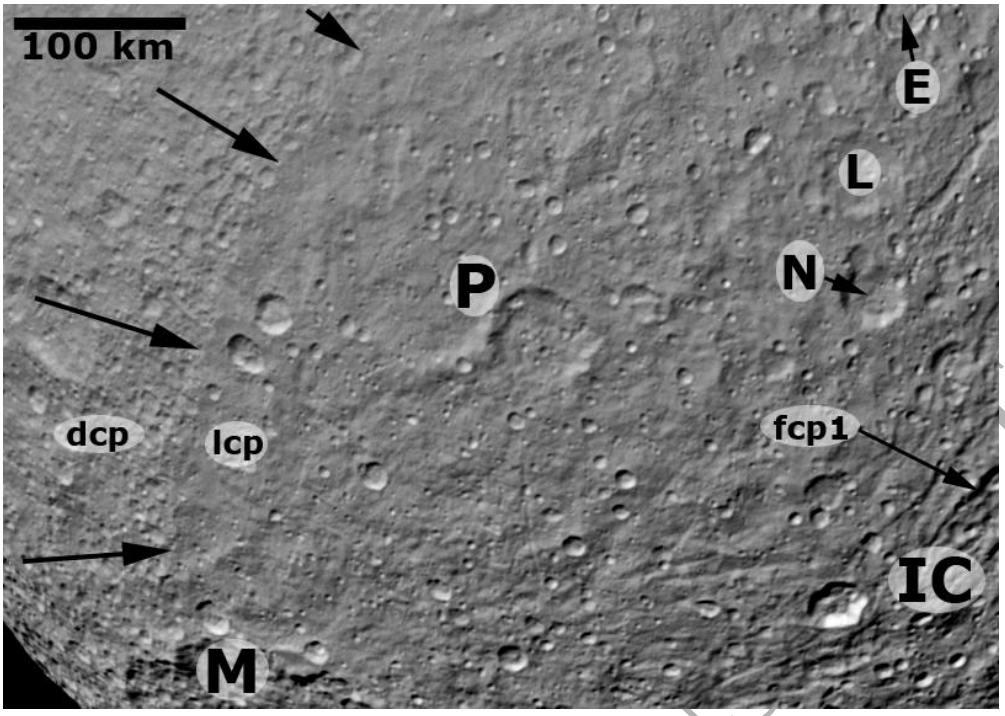

Figure 5

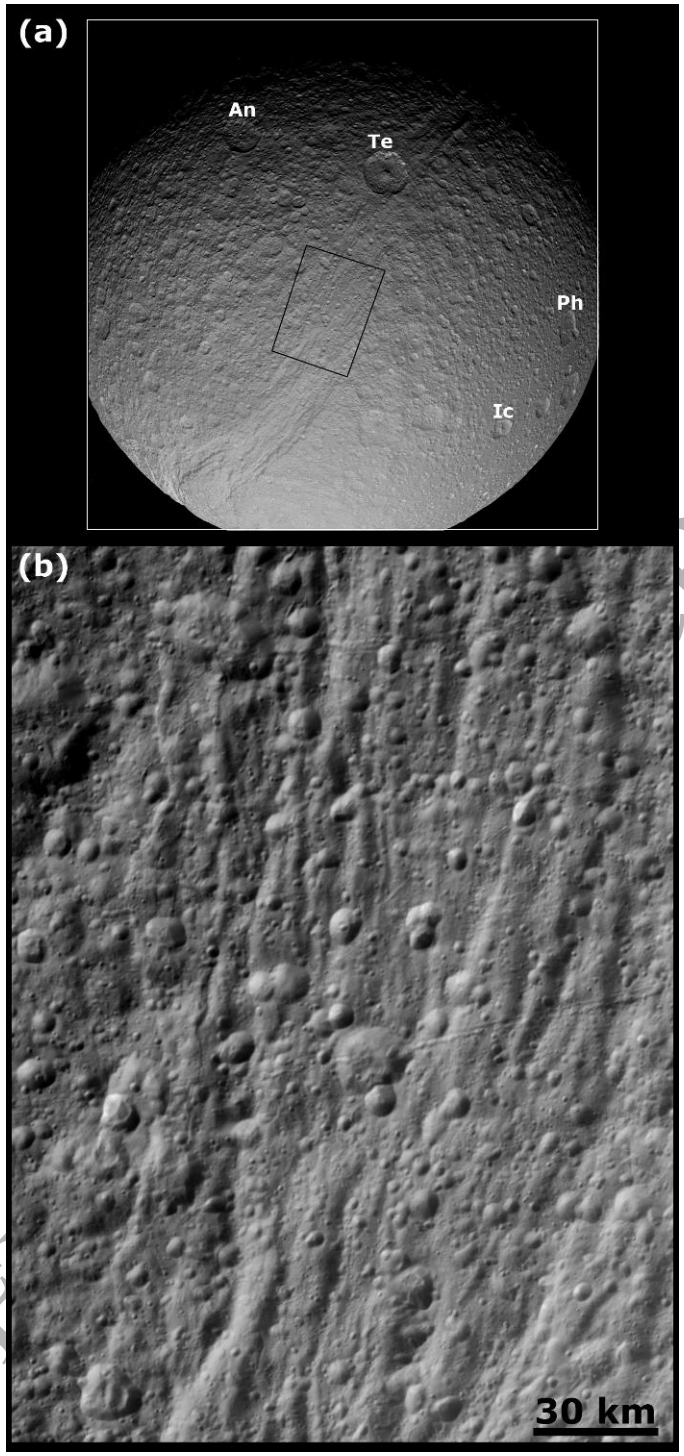

Figure 6

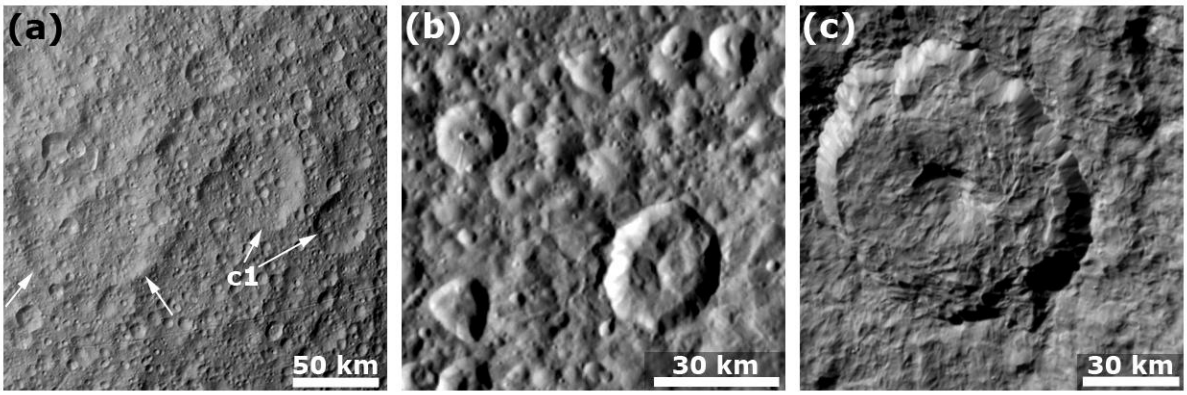

Figure 7

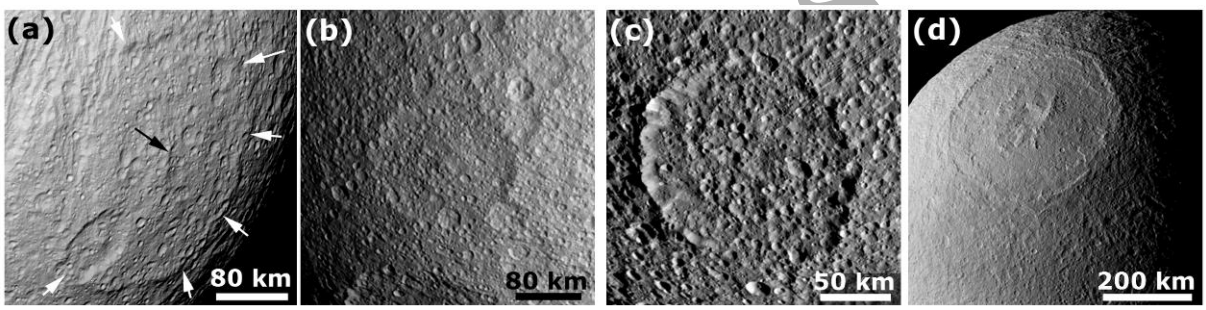

Figure 8

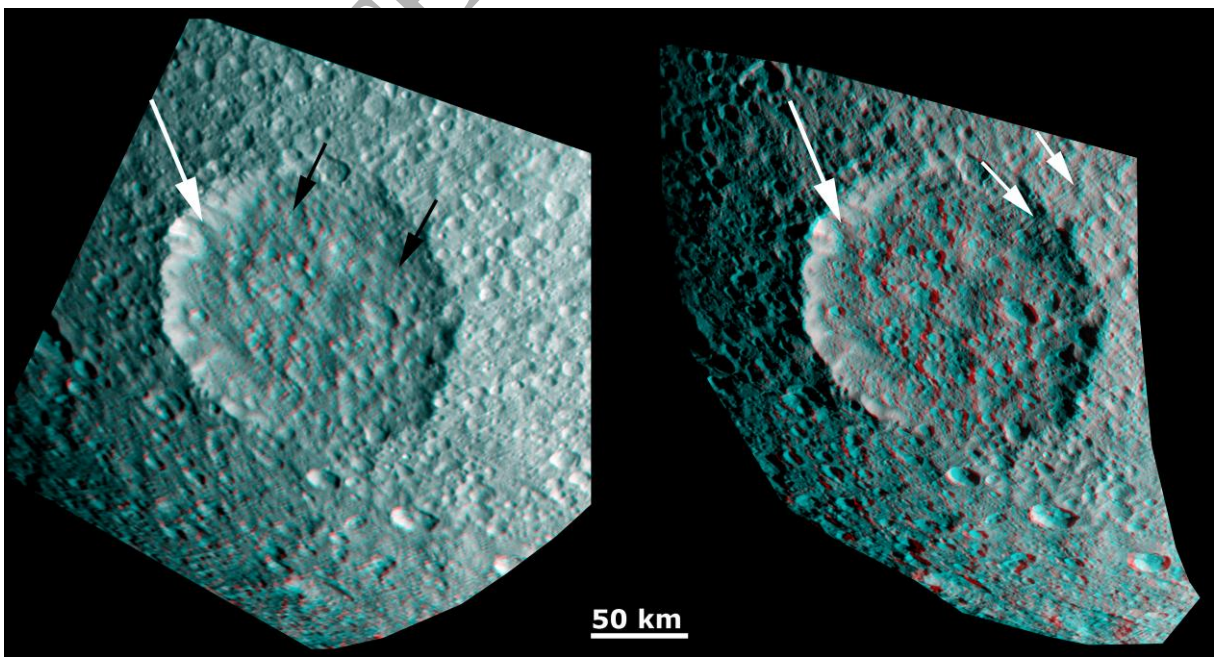

[Figure 9]

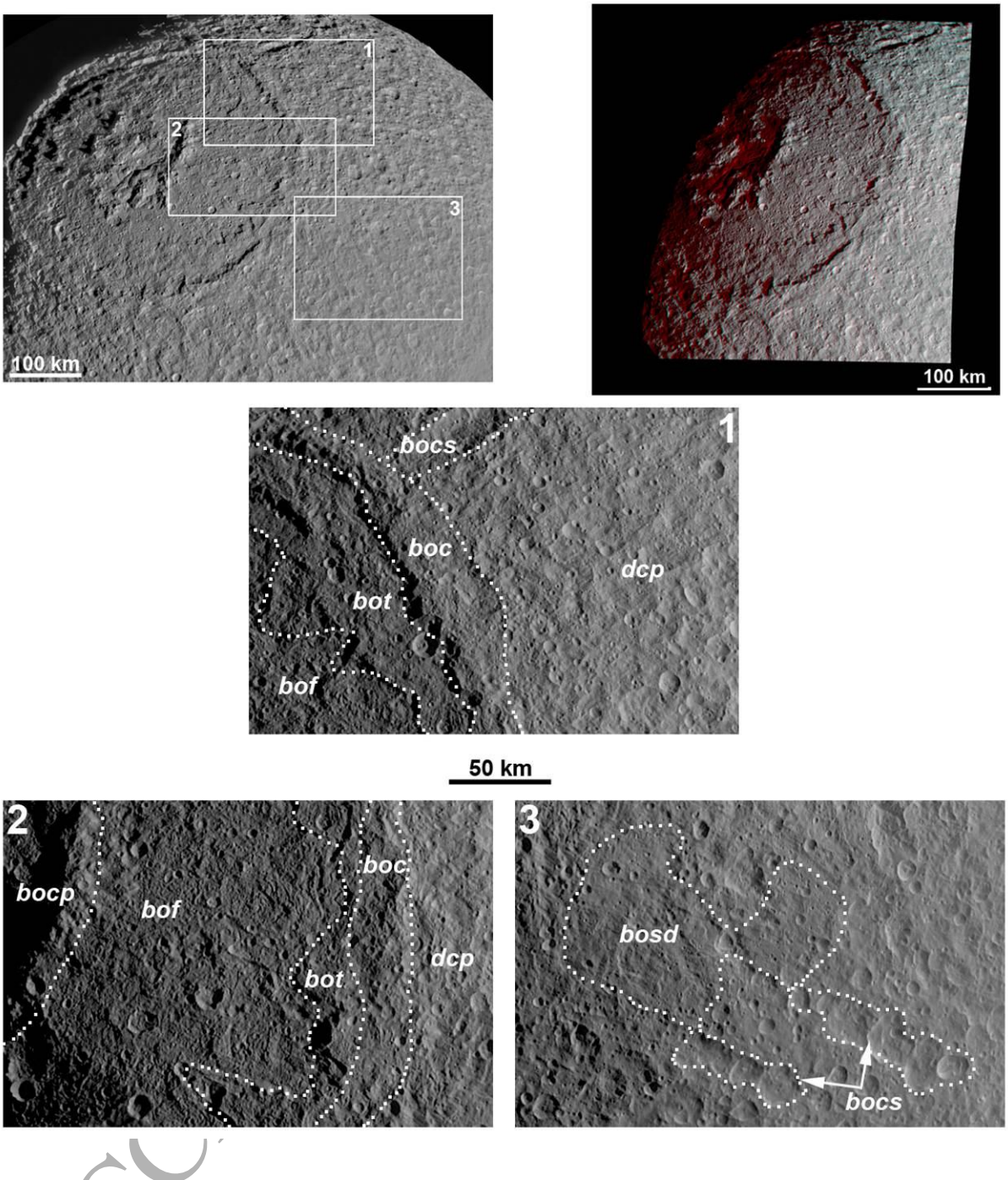
1
2
3
100 km
100 km
bocs
boc
dcp
bot
bof
50 km
2
bocp
bof
boc
dcp
bot
3
bosd
bocs

[Figure 10]

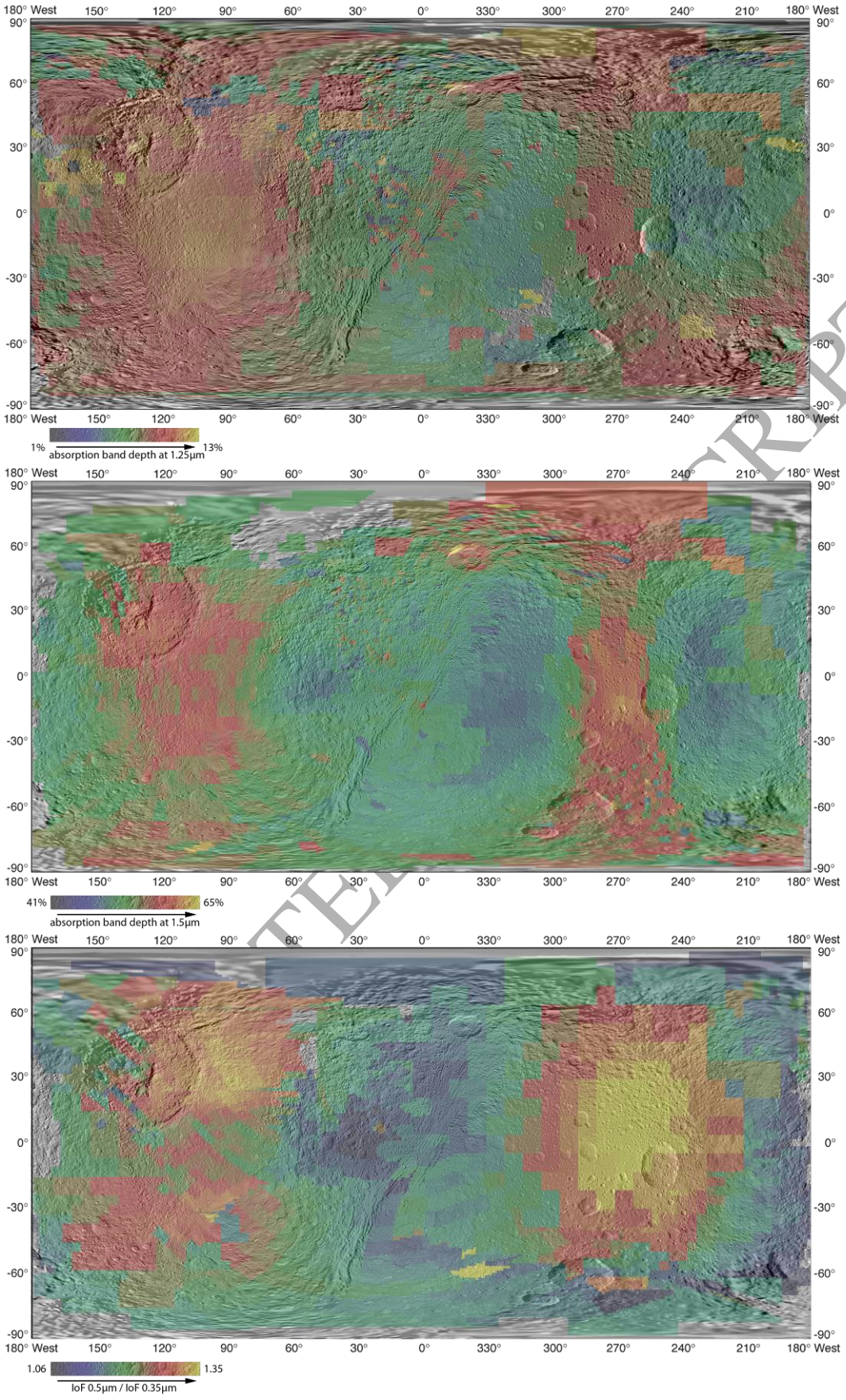
180° West 150° 120° 90° 60° 30° 0° 330° 300° 270° 240° 210° 180° West
90°
60°
30°
0°
-30°
-60°
-90°
1%
absorption band depth at 1.25µm
13%
41%
absorption band depth at 1.5µm
65%
1.06
IoF 0.5µm / IoF 0.35µm
1.35

[Figure11]

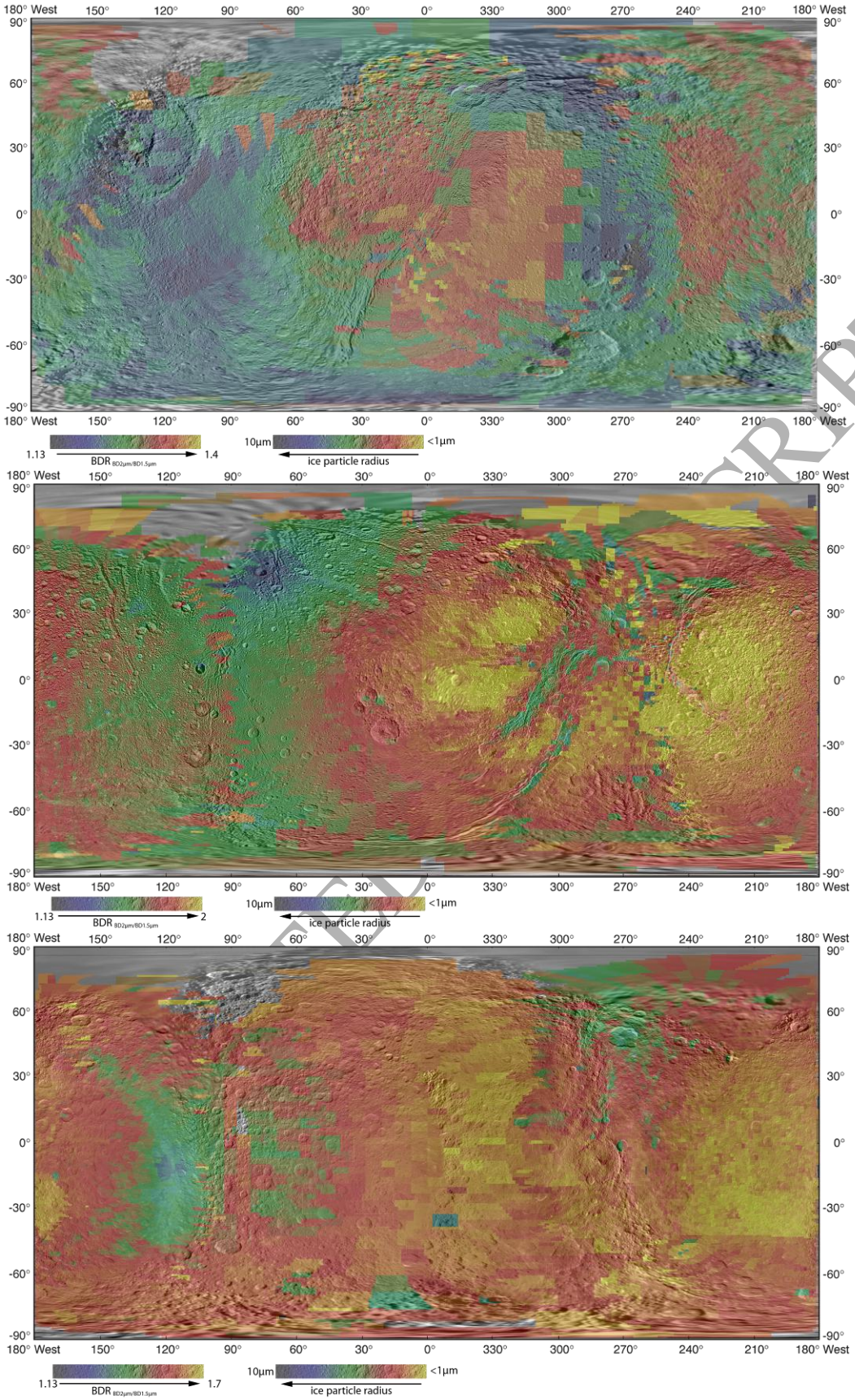
180° West 150° 120° 90° 60° 30° 0° 330° 300° 270° 240° 210° 180° West
90° 60° 30° 0° -30° -60° -90°
1.13 BDR BD2μm/BD1.5μm 1.4
10μm <1μm ice particle radius
1.13 BDR BD2μm/BD1.5μm 2
10μm <1μm ice particle radius
1.13 BDR BD2μm/BD1.5μm 1.7
10μm <1μm ice particle radius

[Figure 12]

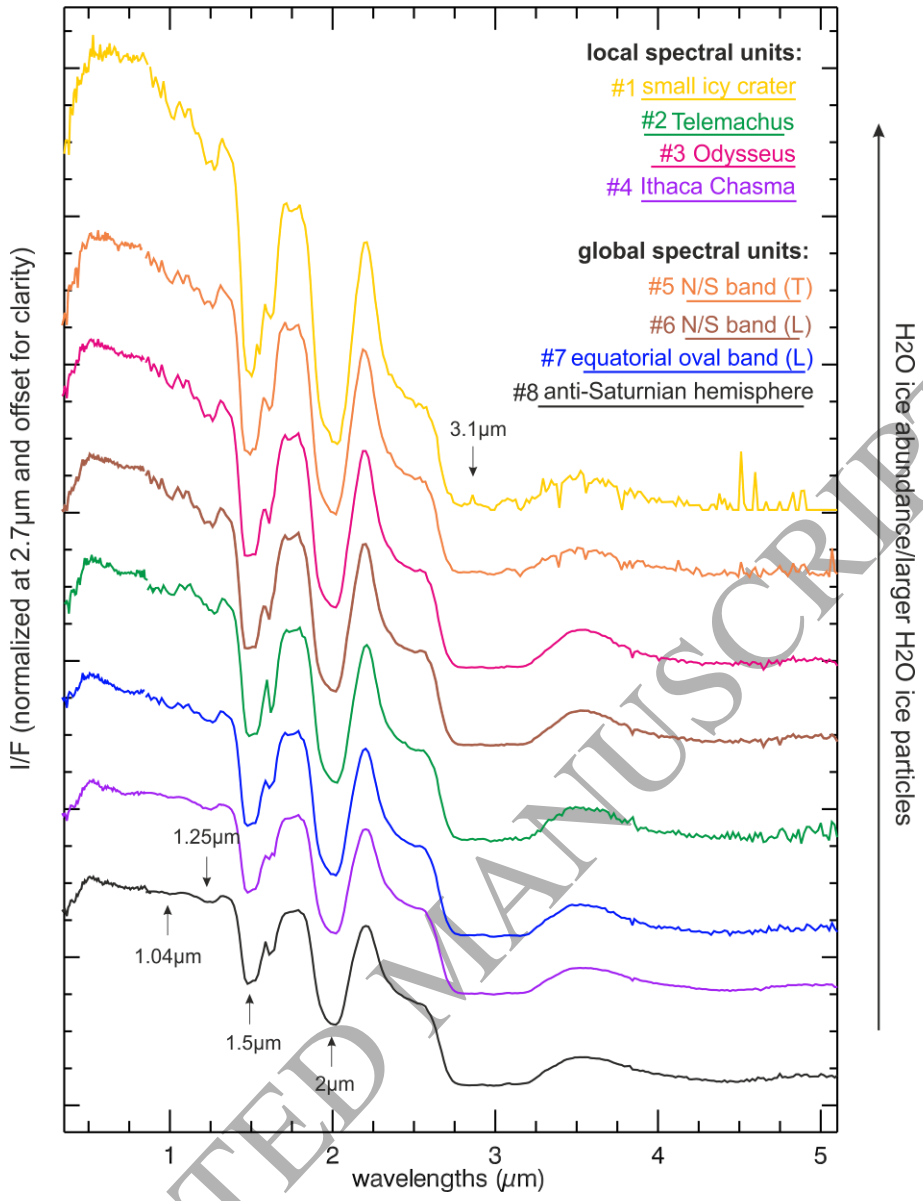

[Figure 13]

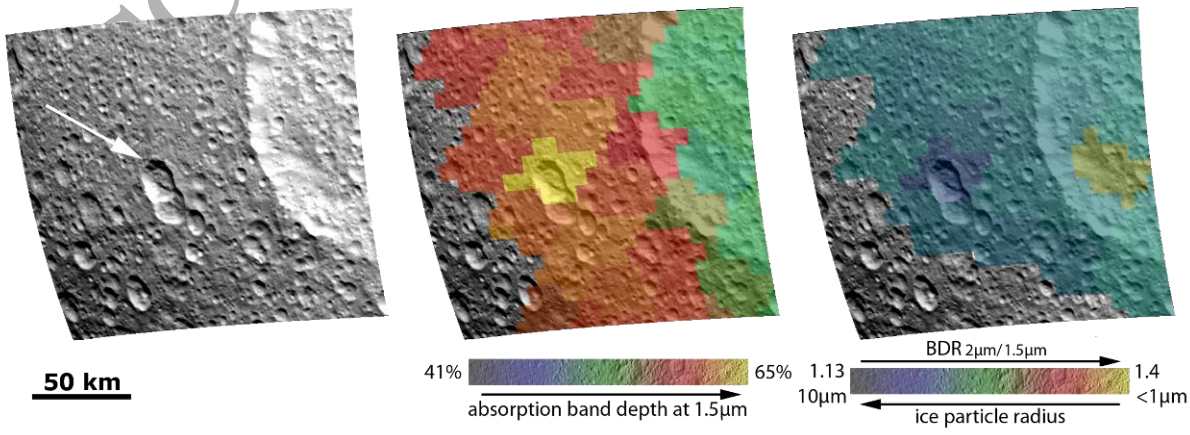

[Figure14]

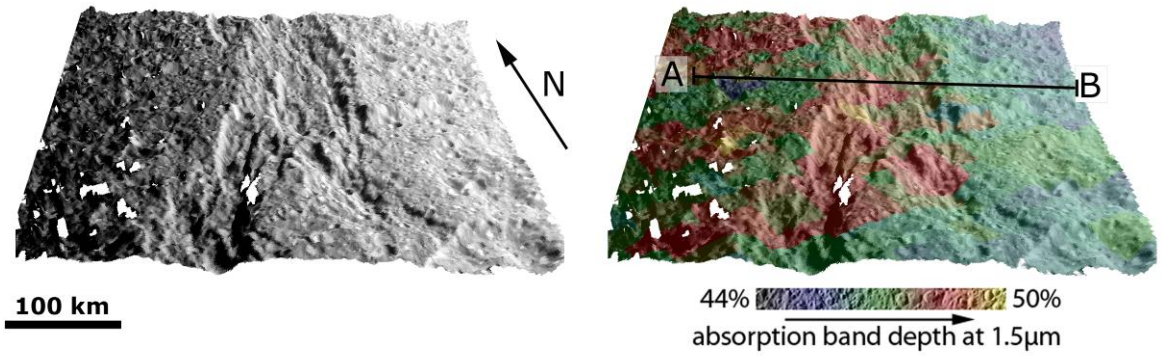

[Figure 15]

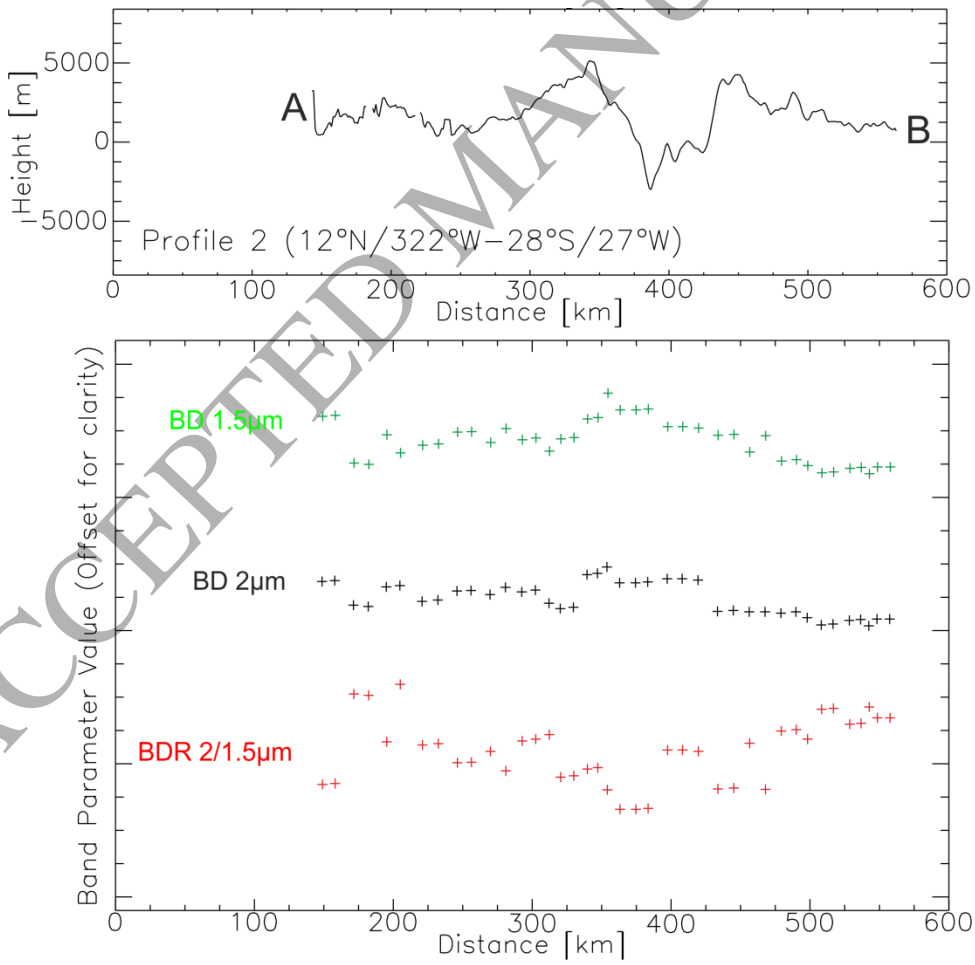

[Figure 16]

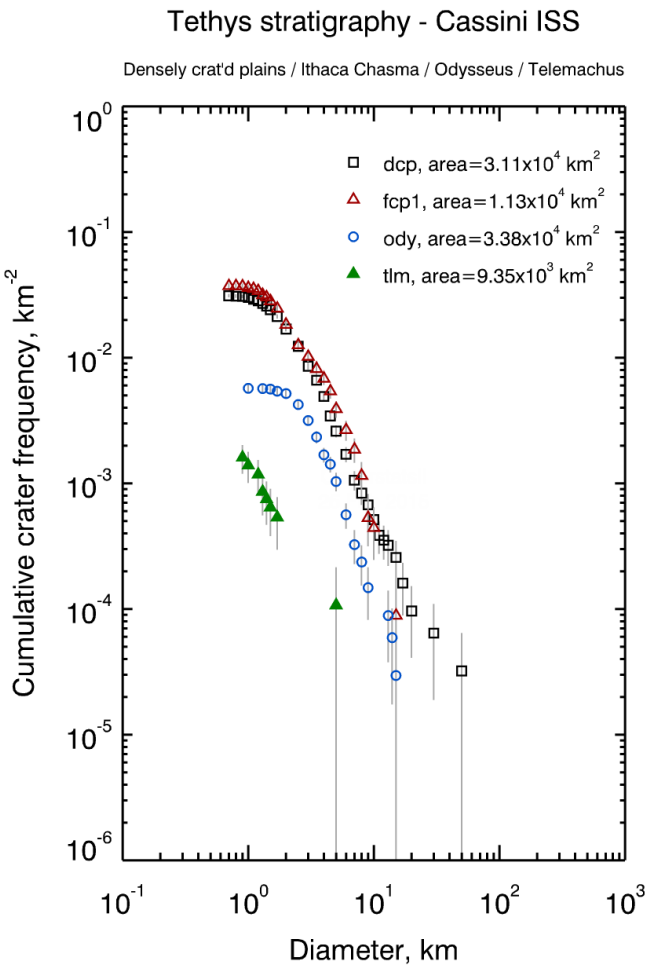
Tethys stratigraphy - Cassini ISS
Densely crat'd plains / Ithaca Chasma / Odysseus / Telemachus
dcp, area=3.11x10^4 km^2
fcp1, area=1.13x10^4 km^2
ody, area=3.38x10^4 km^2
tlm, area=9.35x10^3 km^2
Cumulative crater frequency, km^-2
Diameter, km

[Figure 17]

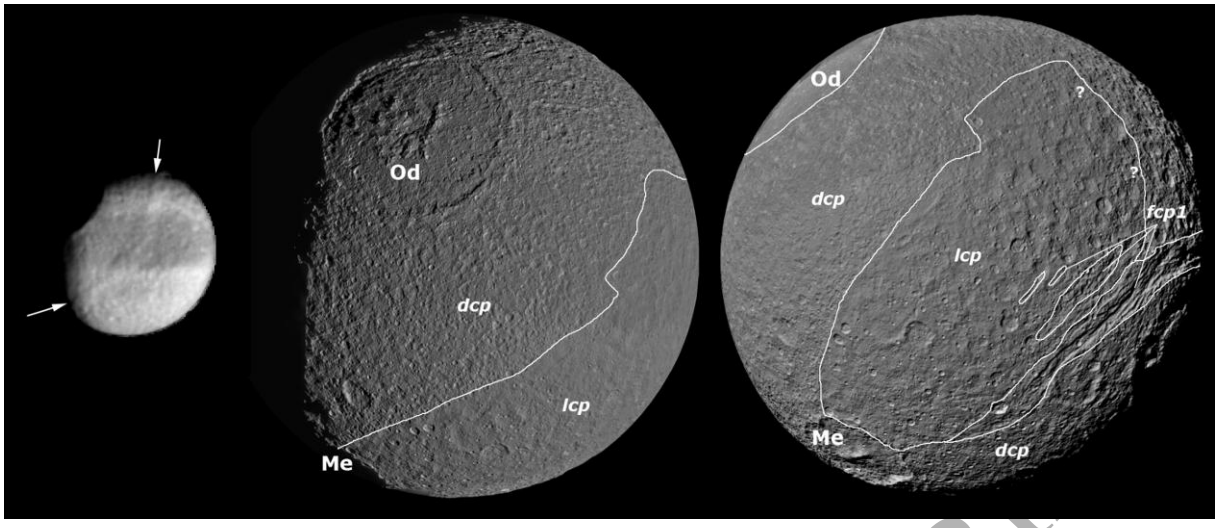

[Figure 18]

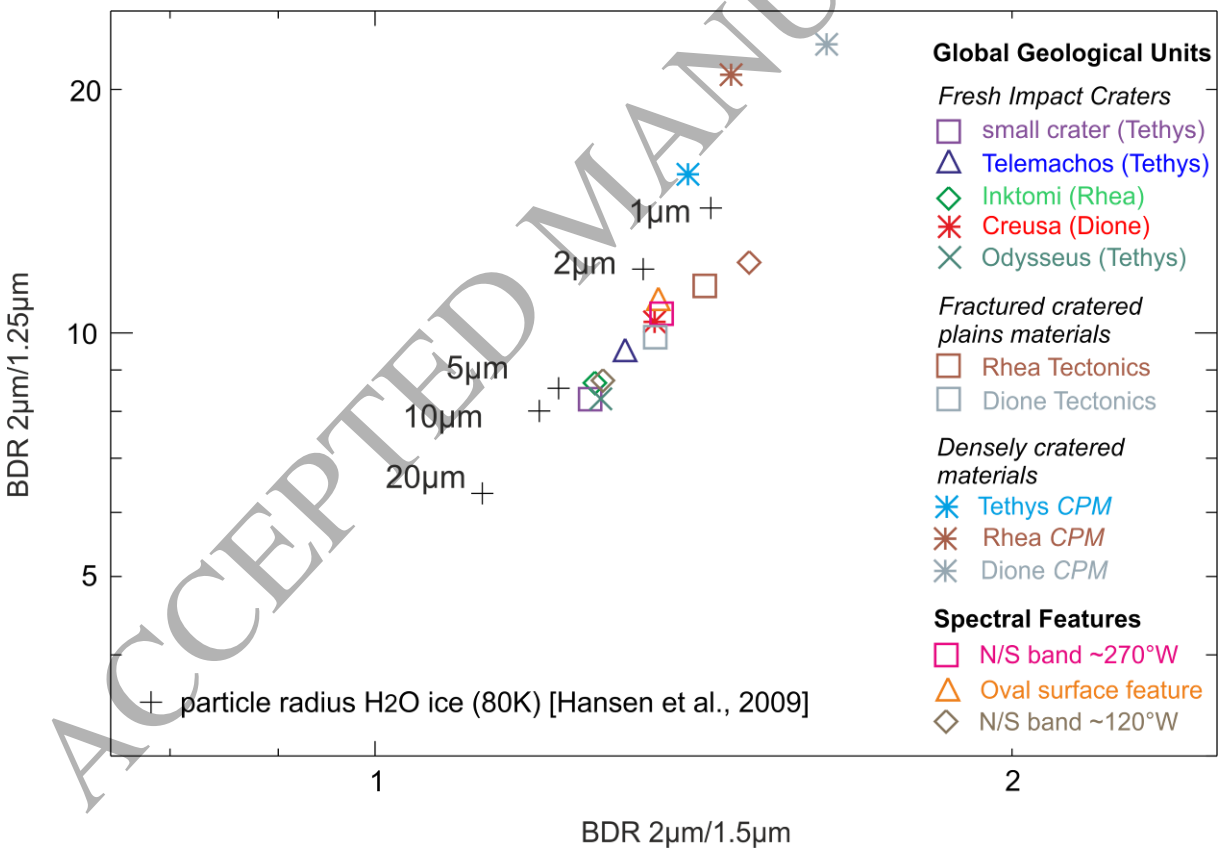

[Figure 19]

11 References

Brown, R. H., et al. (2004), The Cassini Visual And Infrared Mapping Spectrometer (Vims) Investigation, *Space Sci. Rev.*, *115*(1-4), 111-168.
Buratti, B. J., and J. Veverka (1984), Voyager photometry of Rhea, Dione, Tethys, Enceladus and Mimas, *Icarus*, *58*(2), 254-264.
Buratti, B. J., J. A. Mosher, and T. V. Johnson (1990), Albedo and color maps of the Saturnian satellites, *Icarus*, *87*(2), 339-357.
Buratti, B. J., J. A. Mosher, P. D. Nicholson, C. A. McGhee, and R. G. French (1998), Near-Infrared Photometry of the Saturnian Satellites during Ring Plane Crossing, *Icarus*, *136*(2), 223-231.
Chen, E. M. A., and F. Nimmo (2008), Implications from Ithaca Chasma for the thermal and orbital history of Tethys, *Geophysical Research Letters*, *35*, 19203.
Clark, R. N., G. A. Swayze, K. E. Livo, R. F. Kokaly, S. J. Sutley, J. B. Dalton, R. R. McDougal, and C. A. Gent (2003), Imaging spectroscopy: Earth and planetary remote sensing with the USGS Tetracorder and expert systems, *J. Geophys. Res.*, *108*(E12), 44.
Clark, R. N., et al. (2008), Compositional mapping of Saturn's satellite Dione with Cassini VIMS and implications of dark material in the Saturn system, *Icarus*, *193*(2), 372-386.
Clark, R. N., et al. (2012), The surface composition of Iapetus: Mapping results from Cassini VIMS, *Icarus*, *218*, 831-860.
Cruikshank, D. P., et al. (2007), Surface composition of Hyperion, *Nature*, *448*(7149), 54-56.
Dones, L., C. R. Chapman, W. B. McKinnon, H. J. Melosh, M. R. Kirchoff, G. Neukum, and K. J. Zahnle (2009), Icy Satellites of Saturn: Impact Cratering and Age Determination

Saturn from Cassini-Huygens, edited by M. K. Dougherty, L. W. Esposito and S. M. Krimigis, pp. 613-635, Springer Netherlands.
Dozier, J. (1989), Remote Sensing of snow in visible and near-infrared wavelengths, in *Theory and Applications of optical remote sensing*, edited by G. Asrar, pp. 527 - 547, John Wiley & Sons.
Emery, J. P., D. M. Burr, D. P. Cruikshank, R. H. Brown, and J. B. Dalton (2005), Near-infrared (0.8-4.0 μm) spectroscopy of Mimas, Enceladus, Tethys, and Rhea, *Astronomy and Astrophysics*, *435*(1), 353-362.
Filacchione, G., et al. (2010), Saturn's icy satellites investigated by Cassini–VIMS, *Icarus*, *206*(2), 507-523.
Filacchione, G., et al. (2012), Saturn's icy satellites and rings investigated by Cassini-VIMS: III - Radial compositional variability, *Icarus*, *220*, 1064-1096.
Filacchione, G., et al. (2007), Saturn's icy satellites investigated by Cassini-VIMS: I. Full-disk properties: 350-5100 nm reflectance spectra and phase curves, *Icarus*, *186*(1), 259-290.
Giese, B., R. Wagner, G. Neukum, P. Helfenstein, and P. C. Thomas (2007), Tethys: Lithospheric thickness and heat flux from flexurally supported topography at Ithaca Chasma, *Geophysical Research Letters*, *34*(21).
Giese, B., T. Denk, G. Neukum, T. Roatsch, P. Helfenstein, P. C. Thomas, E. P. Turtle, A. McEwen, and C. C. Porco (2008), The topography of Iapetus' leading side, *Icarus*, *193*(2), 359-371.
Grundy, W. M., and B. Schmitt (1998), The temperature-dependent near-infrared absorption spectrum of hexagonal <formula>H2O ice, *Journal of Geophysical Research*, *103*, 25809-25822.
Hansen, G. B. (2009), Calculation of single-scattering albedos: Comparison of Mie results with Hapke approximations, *Icarus*, *203*, 672-676.

Hansen, G. B., and T. B. McCord (2004), Amorphous and crystalline ice on the Galilean satellites: A balance between thermal and radiolytic processes, *Journal of Geophysical Research*, *109*(E1).
Hansen, G. B., E. C. Hollenbeck, K. Stephan, S. K. Apple, and E.-J. Z. Shin-White (2012), Water ice abundance and CO2 band strength on the saturnian satellite Phoebe from Cassini/VIMS observations, *Icarus*, *220*(2), 331-338.
Hansen, G. B., et al. (2005), Ice Grain Size Distribution: Differences Between Jovian and Saturnian Icy Satellites From Galileo and Cassini Measurements, in *American Geophysical Union, Fall Meeting 2005*, edited.
Howett, C. J. A., J. R. Spencer, T. Hurford, A. Verbiscer, and M. Segura (2012), PacMan returns: An electron-generated thermal anomaly on Tethys, *Icarus*, *221*, 1084-1088.
Hurford, T. A., A. R. Sarid, and R. Greenberg (2007), Cycloidal cracks on Europa: Improved modeling and non-synchronous rotation implications, *Icarus*, *186*(1), 218-233.
Jaumann, R., R. N. Clark, F. Nimmo, A. R. Hendrix, B. J. Buratti, T. Denk, J. M. Moore, P. M. Schenk, S. J. Ostro, and R. Srama (2009), Icy Satellites: Geological Evolution and Surface Processes, in *Saturn from Cassini-Huygens*, edited by M. K. Dougherty, L. W. Esposito and S. M. Krimigis, pp. 637-681, Springer Netherlands.
Jaumann, R., et al. (2008), Distribution of icy particles across Enceladus' surface as derived from Cassini-VIMS measurements, *Icarus*, *193*(2), 407-419.
Jaumann, R., et al. (2006), High-resolution CASSINI-VIMS mosaics of Titan and the icy Saturnian satellites, *Planetary and Space Science*, *54*(12), 1146-1155.
Kirchoff, M. R., and P. Schenk (2010), Impact cratering records of the mid-sized, icy saturnian satellites, *Icarus*, *206*(2), 485-497.
McCord, T. B., G. B. Hansen, J. H. Shirley, and R. W. Carlson (1999), Discussion of the 1.04-μm water ice absorption band in the Europa NIMS spectra and a new NIMS calibration, *Journal of Geophysical Research*, *104*, 27157-27162.
Moore, and J. L. Ahern (1983), The geology of Tethys, *J. Geophys. Res.*, *88*(S2), A577-A584.
Moore, J. M., and P. M. Schenk (2007), Topography of endogenic features on Saturnian mid-sized satellites, *Lunar Planet. Sci. Conf. XXXVIII*, *1338*.
Moore, J. M., P. M. Schenk, L. S. Bruesch, E. Asphaug, and W. B. McKinnon (2004), Large impact features on middle-sized icy satellites, *Icarus*, *171*(2), 421-443.
Moore, J. M., and Ahern, J. L. (1983), The geology of Tethys, *J. Geophys. Res.*, *88*, A577-A584.
Multhaup, K., and T. Spohn (2007), Stagnant lid convection in the mid-sized icy satellites of Saturn, *Icarus*, *186*, 420-435.
Neukum, G., R. Wagner, T. Denk, and C. C. Porco (2006), Cratering Chronologies and Ages of the Major Saturnian Satellites, *Geophysical Research Abstracts*, *8*(09252).
Neukum, G., J. Oberst, H. Hoffmann, R. Wagner, and B. A. Ivanov (2001), Geologic evolution and cratering history of Mercury, *Planetary and Space Science*, *49*, 1507-1521.
Plescia, J. B., and J. M. Boyce (1982), Crater densities and geological histories of Rhea, Dione, Mimas and Tethys, *Nature*, *295*(5847), 285-290.
Plescia, J. B., and J. M. Boyce (1985), Impact Cratering History of the Saturnian Satellites, *J. Geophys. Res.*, *90*(B2), 2029-2037.
Porco, C. C., et al. (2004), Cassini Imaging Science: Instrument Characteristics And Anticipated Scientific Investigations At Saturn, *Space Science Reviews*, *115*(1), 363-497-497.
Roatsch, T., et al. (2009), High-resolution Atlases of Mimas, Tethys, and Iapetus derived from Cassini-ISS images, *Planetary and Space Science*, *57*, 83-92.
Schenk, P., and J. Moore (2009), Eruptive Volcanism on Saturn's Icy Moon Dione, in *Lunar and Planetary Science Conference*, edited, p. 2465.

Schenk, P., D. P. Hamilton, R. E. Johnson, W. B. McKinnon, C. Paranicas, J. Schmidt, and M. R. Showalter (2011), Plasma, plumes and rings: Saturn system dynamics as recorded in global color patterns on its midsize icy satellites, *Icarus*, *211*(1), 740-757.
Schmedemann, N., T. Kneissl, A. Neesemann, G. Michael, R. J. Wagner, C. A. Raymond, and C. T. Russell (2014), The Signature of Secondary Cratering on 4 Vesta and Tethys, in *Lunar and Planetary Science Conference*, edited, p. 1960.
Smith, B. A., et al. (1981), Encounter with Saturn: Voyager 1 Imaging Science Results, *Science*, *212*(4491), 163-191.
Smith, B. A., et al. (1982), A New Look at the Saturn System: The Voyager 2 Images, *Science*, *215*(4532), 504-537.
Spudis, P. D. (1993), *The Geology of Multi-ring Impact Basins*.
Stephan, K. (2006), Chemisch-physikalische Zusammensetzung der Ganymedoberfläche: Zusammenhänge mit geologischen Strukturen und deren Gestaltungsprozessen, PhD. Dissertation (in german) thesis.
Stephan, K., C. A. Hibbitts, G. B. Hansen, and R. Jaumann (2011), Comparison of variations in ice particle sizes across Callisto's and Ganymede's surface, paper presented at EPSC-DPS Joint Meeting, Nantes.
Stephan, K., R. Jaumann, R. Wagner, and J. Castillo-Rogez (2013), Geology of Icy Bodies, in *The Science of Solar System Ices*, edited by M. S. Gudipati, p. 279.
Stephan, K., C. A. Hibbitts, R. Wagner, R. Jaumann, and G. B. Hansen (2009), Ganymede's spectral properties: implications for further investigations in a future mission to Jupiter and its satellites, *European Planetary Science Congress*, *4*

EPSC2009-2633.
Stephan, K., et al. (2014), Small fresh impact craters on asteroid 4 Vesta: A compositional and geological fingerprint, *Journal of Geophysical Research (Planets)*, *119*, 771-797.
Stephan, K., et al. (2010), Dione's spectral and geological properties, *Icarus*, *206*(2), 631-652.
Stephan, K., et al. (2012), The Saturnian satellite Rhea as seen by Cassini VIMS, *Planetary and Space Science*, *61*(1), 142-160.
Stooke, P. J. (1989), Tethys: Volcanic and Structural Geology, *Abstracts of the Lunar and Planetary Science Conference*, *20*, 1071.
Stooke, P. J. (2002), Tethys and Dione: New Geological Interpretations, in *Lunar Planet. Sci. Conf. XXXIII*, edited, Houston, Texas.
Teolis, B. D., et al. (2010), Cassini finds an oxygen-carbon dioxide atmosphere at Saturn's icy moon Rhea, *Science*, *330*(6012), 1813-1815.
Thomas, P. C. (2010), Sizes, shapes, and derived properties of the saturnian satellites after the Cassini nominal mission, *Icarus*, *208*, 395-401.
Verbiscer, A., R. French, M. Showalter, and P. Helfenstein (2007), Enceladus: Cosmic Graffiti Artist Caught in the Act, *Science*, *315*(5813), 815.
Wagner, K. Stephan, N. Schmedemann, T. Roatsch, E. Kersten, G. Neukum, and C. C. Porco (2013a), Regional geology and stratigraphy of Saturn's icy moon Tethys, in *EGU General Assembly Conference Abstracts*, edited, p. 11009.
Wagner, K. Stephan, N. Schmedemann, T. Roatsch, E. Kersten, G. Neukum, and C. C. Porco (2013b), Geologic Evolution of Saturn's Icy Moon Tethys, in *AAS/Division for Planetary Sciences Meeting Abstracts*, edited.
Wagner, R., G. Neukum, N. Schmedemann, T. Roatsch, T. Denk, and C. C. Porco (2012), Clusters of craters on the Saturnian satellite Dione: morphology and size distribution, in *European Planetary Science Congress 2012*, edited, p. 888.
Wilhelms, D. E. (1990), Geologic Mapping, in *Planetary Mapping*, edited by R. Greeley, p. 208.
Zahnle, K., P. Schenk, H. Levison, and L. Dones (2003), Cratering rates in the outer solar system, *Icarus*, *163*, 263–289.

Zhang, K., and F. Nimmo (2012), Late-stage impacts and the orbital and thermal evolution of Tethys, *Icarus*, *218*(1), 348-355.